Annu. Rev. Phys. Chem. 1998. 49:441–80

OPTICAL STUDIES OF SINGLE MOLECULES AT ROOM TEMPERATURE

X. Sunney Xie
Pacific Northwest National Laboratory, Environmental Molecular Sciences Laboratory, PO Box 999, K8-88, Richland, Washington 99352; e-mail: xsxie@pnl.gov

Jay K. Trautman
SEQ Ltd, 17 Princess Road, Lawrenceville, New Jersey 08648;
e-mail: jtrautman@seqltd.com

KEY WORDS: single-molecule detection, single-molecule spectroscopy, single-molecule dynamics, fluorescence microscopy

ABSTRACT

Recent developments in optical studies of single molecules at room temperature are reviewed, with an emphasis on the underlying principles and the potential of single-molecule experiments. Examples of single-molecule studies are given, including photophysics and photochemistry pertinent to single-molecule measurements, spectral fluctuations, Raman spectroscopy, diffusional motions, conformational dynamics, fluorescence resonant energy transfer, exciton dynamics, and enzymatic turnovers. These studies illustrate the information obtainable with the single-molecule approach that is hidden in ensemble-averaged measurements.

INTRODUCTION

In chemistry texts, molecular interactions and chemical reactions are generally described on a single-molecule basis. However, our knowledge of molecular interactions and chemical dynamics has come almost exclusively from experiments on ensembles of molecules. For years scientists have sought methods to probe the behavior of single molecules. The most notable successes have been the single–ion-channel recording with the patch-clamp technique (1) and the visualization of single atoms and molecules with scanning tunneling

0066-426X/98/1001-0441$08.00

and atomic force microscopy (2, 2a). Recent advances in optical spectroscopy and microscopy have made it possible not only to detect and image single molecules, but to conduct spectroscopic measurements and monitor dynamic processes as well. Optical spectroscopy is a powerful method for studying chemical species and their interactions with the environment. In addition, optical measurements afford the time resolution required to monitor many dynamic processes. Single-molecule studies are beginning to impact a number of disciplines, including analytical chemistry, material research, and the biological sciences. In this chapter, we review recent developments in optical studies of single molecules at room temperature. [This restriction excludes the pioneering low-temperature work, which has been reviewed recently (3–5).] We give only cursory treatment to experimental techniques that have been adequately covered in earlier reviews of room-temperature single-molecule work (6–10) and, instead, emphasize the underlying principles of single-molecule experiments and the information obtained from them.

It is generally accepted that single-molecule measurements represent a technological breakthrough with possible practical applications, but whether any new information can be obtained has been questioned. A fundamental postulate of statistical mechanics, the ergodic hypothesis, states that the time-average of a physical quantity along the trajectory of a member of the ensemble is equivalent to the average of that quantity at a given time over the ensemble. Why, then, follow one member for a period of time when it is possible to gather the equivalent information by sampling the entire ensemble at once? For the ergodic hypothesis to be even approximately applicable, the ensemble must consist of entirely equivalent members, i.e. it must be homogeneous. However, many chemical and biological systems are inhomogeneous. The inhomogeneity can be truly static, or as a practical equivalence, the measurement time can be shorter than the relevant fluctuations. Whatever the origin, in an inhomogeneous system, the trajectory average varies among the members of the ensemble and is no longer equivalent to the ensemble average.

The significance of single-molecule experiments is twofold. First, for inhomogeneous systems, there is often no a priori knowledge of the distribution of a given molecular property. Ensemble-averaged measurements can be used to determine the mean value of a quantity but cannot generally be used to determine the distribution of the quantity. Without the distribution, the behavior of individual members of the ensemble cannot be deduced. Examples of single-molecule measurements that allow the distributions of molecular properties to be determined are given throughout the chapter, as are examples of experiments that permit correlations among properties to be deduced. Second, single-molecule trajectories are direct records of the fluctuations that contain detailed dynamical and statistical information. This is true, of course, for both homogeneous and

inhomogeneous systems. Even in the case of a homogeneous system, analyses of trajectories are more informative than are ensemble-averaged results. The power of trajectory analysis has been demonstrated in molecular dynamics simulations that are also single-molecule experiments (11). Although single-molecule fluorescence measurements do not allow the recording of trajectories on the timescale of molecular dynamics simulations (femtosecond to nanosecond), they can be obtained on the millisecond to tenth-second timescale, as we illustrate with translational, orientational, spectral, and enzymatic-turnover trajectories.

The inaccessibility of the nanosecond timescale in single-molecule trajectory measurements is due to the requirement, imparted by signal-to-noise considerations, of repetitive excitation, each cycle of which occurs maximally on the nanosecond timescale. Fluorescence lifetimes of single molecules can nevertheless be measured with picosecond resolution using time-correlated photon counting. The measured lifetime is an averaged quantity, the averaging period being milliseconds or longer, depending on the experiment. Such measurements allow protein motions, photoinduced electron transfer, and fluorescence resonant energy transfer to be probed on single molecules.

One caveat in any single-molecule measurement is that repetitive excitation may create photoinduced artifacts associated with relatively rare photophysical and photochemical processes. Understanding the photophysics and photochemistry pertinent to the experiment is crucial in the extraction of useful information. Of these processes, the most obvious event in a single-molecule trajectory is the one that ends it, namely the irreversible photochemical bleaching of the chromophore. Photobleaching often causes difficulty in the recording of long trajectories.

SINGLE-MOLECULE OPTICAL MEASUREMENTS

Single-molecule spectroscopy was first demonstrated at cryogenic temperatures (3), utilizing the narrow linewidth of the zero-phonon line and the corresponding enormous absorption cross-section of pentacene. A relatively rigid structure is required for a molecule to have a large Franck-Condon factor for the zero-phonon line, and even in this case, the zero-phonon line is broadened and depopulated substantially above 10K. As a result, a limited number of molecules have been explored by single-molecule spectroscopy at cryogenic temperatures. Independently, efforts based on flow cytometry (12), confocal fluorescence correlation spectroscopy (13), and micro-droplets (14) evolved to the level of single-molecule sensitivity at room temperature. However, it was not until the advent of single-molecule imaging with near-field microscopy (15) that the sensitivity was high enough to conduct single-molecule spectroscopic

and dynamic measurements at room temperature (16–18). More recent measurements, which dispensed with the near-field probe, have improved the sensitivity and ease of measurement on immobilized molecules (19). The incorporation of a charge-coupled device (CCD) camera with either total internal reflection (20) or bright field illumination (21) has allowed two-dimensional and even three-dimensional (22) tracking of moving single fluorophores with high time resolution. Presently, any photostable molecule with an extinction coefficient larger than $\sim 10^4$ and a fluorescent quantum efficiency greater than ~ 0.1 can be studied. Techniques are still evolving; for example, the latest developments include two-photon fluorescence detection (23) and imaging (24), and surface-enhanced Raman spectroscopy (25, 26) of single molecules.

In Figure 1, near-field (Figures 1*A–C*) and far-field (Figures 1*D–F*) fluorescence images, spectra, and lifetimes are displayed of the same single molecule of 1,1′-dioctadecyl-3,3,3′,3′-tetramethylindocarbocyanine (diI) situated in a thin film of polymethylmethacrylate (PMMA) under ambient conditions. The near-field image was taken with an aluminum-coated optical fiber tip as the excitation source (15, 27) positioned a few nanometers above a raster-scanned sample. The emission was collected through a transmissive substrate with a high numerical aperture objective in a modified fluorescence microscope. The far-field image was taken with the same microscope with the fiber tip removed, the excitation light being focused by the objective lens (28). The near-field image has a full-width-at-half-maximum of 80 nm, determined by the aperture of the fiber tip. Near-field microscopy allows spectroscopic imaging at a resolution beyond the diffraction limit while offering correlation of topographic information with spectroscopic information (by performing force microscopy with the same tip) (27). However, there is a price to pay for these advantages: The metal coating can perturb the optical measurements, mainly the emission lifetime and the fluorescence intensity. The full-width-at-half-maximum of the far-field images is diffraction-limited to approximately half of the wavelength of the light. The much easier far-field measurement is the method of choice for studying behaviors of single, isolated molecules at low concentrations.

Common to the near- and far-field measurements are significant differences in the spectra and lifetimes among nominally identical molecules (Figures 1*G–I* and Figures 1*J–L*). This information, pertinent to understanding the interactions between molecules and particular local environments, is hidden in the ensemble-averaged spectrum (Figure 1*M*) and lifetime (Figure 1*N*). There are two distinct effects: one electromagnetic, for which a macroscopic description suffices, and the other due to intermolecular or intramolecular interactions, which require a microscopic description. The variation in lifetime shown in Figure 1 is due principally to an electromagnetic effect: the dependence of the radiative rate on the orientation of the molecular transition dipole with respect to the dielectric interface (19). There is a secondary electromagnetic effect:

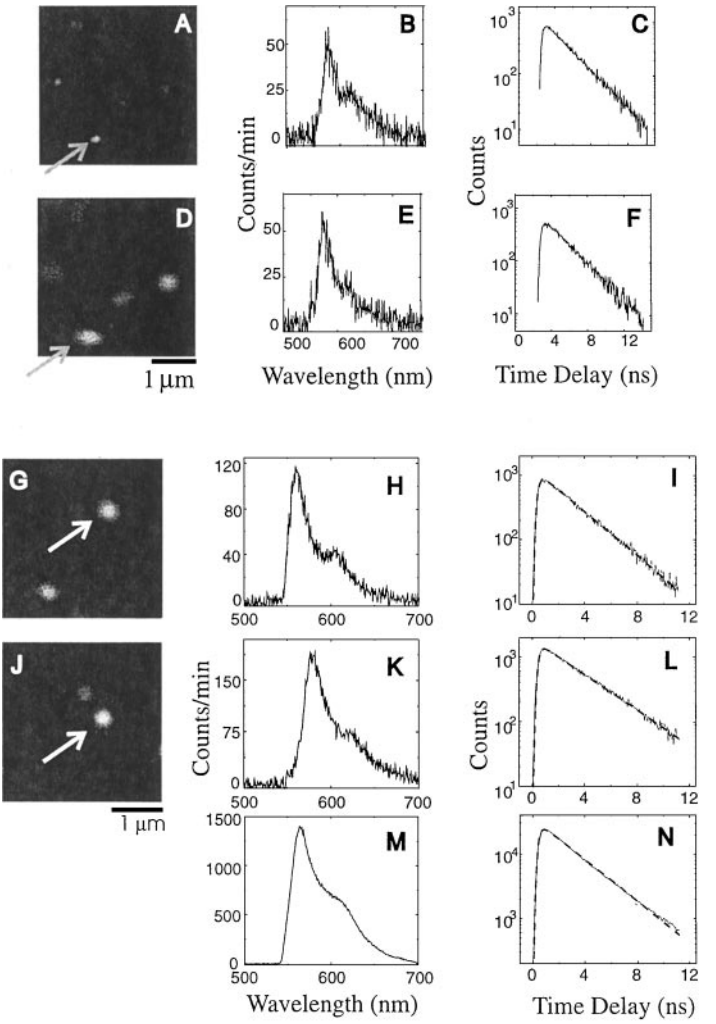

Figure 1 Near-field (*A–C*) and far-field (*D–F*) excited fluorescence images, emission spectra, and excited-state lifetimes obtained from the same 1,1′-dioctadecyl-3,3,3′,3′-tetramethylindocarbocyanine (diI) molecule located at a polymethylmethacrylate-air interface. The excitation flux in the far-field experiment was maintained at a level comparable to that used in the near-field experiment. Note the z-oriented molecules (A, *upper left*). Farfield fluorescence images (*G* and *J*), corresponding spectra (*H* and *K*), and excited-state lifetimes (*I* and *L*) for two diI molecules. The spectrum (*M*) and lifetime (*N*) of an ensemble of hundreds of molecules are included for comparison. An exponential fit to the ensemble lifetime has a value of $\chi^2 = 6.7$, compared with value $\sim$1 for the single-molecule fits, reflecting the distribution of lifetimes in the ensemble. [Reprinted with permission (19, 28).]

The radiative rate goes as the third power of the local-environment-dependent emission frequency (19). Even larger variations of lifetimes are seen in the near-field fluorescence-lifetime measurements because the metal surface can significantly alter both radiative rates and nonradiative (fluorescence-quenching) rates. There have been extensive experimental (17, 18, 28) and theoretical (29, 30) studies on this subject. Because the subject has been reviewed recently (6, 9), we do not dwell on it here. Although the electromagnetic interaction accounts for the variation in radiative rates and fluorescence quenching rates due to dielectric and metallic structures, spectral shifts induced by the electromagnetic interactions are minimal compared with the broad room-temperature spectral width (29). The large spectral variations observed among molecules are due to intermolecular and/or intramolecular interactions.

Another ubiquitous feature of single-molecule measurements is the fluctuation of the experimental observables, such as emission intensity and emission spectrum. Trajectories are never exactly reproducible; only the statistical properties of the trajectories are reproducible. Single-molecule experiments require statistical analysis both within individual trajectories and among a population of molecules. This theme is returned to numerous times below.

Finally, we close this overview by noting that the orientation of single molecular transition dipoles can be completely determined. This was first elegantly demonstrated by Betzig & Chichester with the near-field tip, which possesses a longitudinal E-field component (15). The images of the two molecules in the upper left corner of Figure 1*A* are indicative of a transition dipole orientation substantially perpendicular to the sample plane. In conventional far-field measurements, it is straightforward to determine the in-plane orientation. Moreover, Macklin & Trautman (31) have demonstrated imaging of out-of-plane dipoles with a high numerical aperture objective. This was accomplished with a donut-mode laser beam, for which the longitudinal-field component is comparable to (actually slightly larger than) the transverse-field component at the focus. Figure 2*A* shows the calculated field components of a focused Hermite-Gaussian beam. Figures 2*B* and *C* are the fluorescence images and lifetimes of two molecules with transition dipoles substantially perpendicular to the sample plane (Figure 2*B*) and in the sample plane (Figure 2*C*), respectively. The lifetimes are consistent with the assigned orientations, as per the experiments of Macklin et al (19).

PHOTOPHYSICS AND PHOTOCHEMISTRY IN SINGLE-MOLECULE MEASUREMENTS

An understanding of basic photophysics and photochemistry is highly pertinent to single-molecule experiments. Upon excitation to the first excited singlet state,

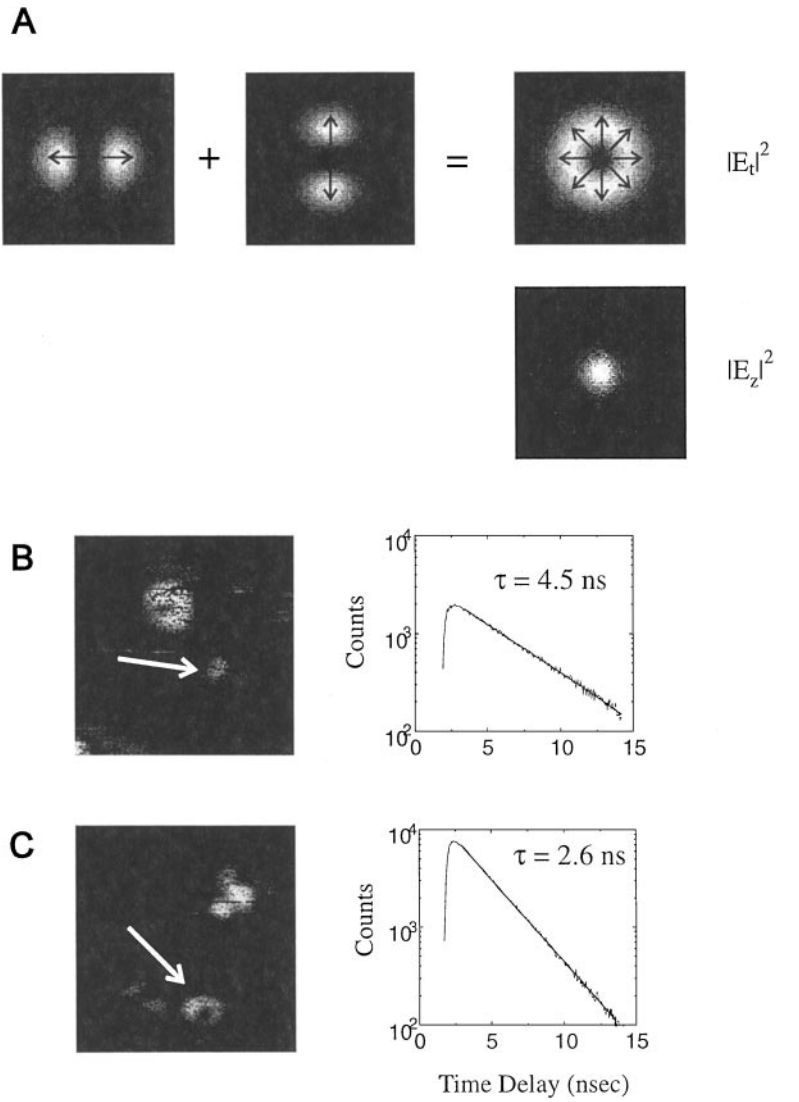

Figure 2 Calculations of the intensity contours of a tightly focused "donut-mode." (*A*) The first set of figures is the transverse field intensity. (*arrows*) The field polarization. The longitudinal-z-field intensity is plotted on the same scale. (*B* and *C*) Fluorescence images and excited-state lifetimes of two 1,1′-dioctadecyl-3,3,3′,3′-tetramethylindocarbocyanine molecules in a thin film of polymethylmethacrylate (PMMA). (*B*) The transition dipole of the molecule (*arrow*) is oriented primarily out-of-plane. (*C*) The molecule is principally in-the-plane. The lifetimes are consistent with the orientations for molecules at a PMMA-air interface (19). (Courtesy of JJ Macklin, SEQ Ltd.)

a molecule has a certain quantum efficiency for intersystem crossing (ISC) to the triplet manifold, ϕ_{ISC}. Typically, ϕ_{ISC} is $\sim 10^{-2}$, although the range is quite large. Thus, during the course of an experiment where the number of excitation-emission cycles is $\sim 10^5$, the molecule will pass through the triplet manifold many times. If the triplet lifetime is longer than the average excitation-emission cycle-time, then the single-molecule emission will be intermittently switched off. This phenomenon has been observed at both low temperature (32) and room temperature (33, 34). Figures 3*A–C* provide a visual demonstration of the effect. In Figure 3*C*, the triplet lifetime is not only longer than the excitation-emission cycle-time, it is also longer than the pixel dwell-time of the raster-scanned image. The kinetics of ISC and the subsequent relaxation of the triplet to the ground state can be easily extracted from an analysis of the single-molecule emission intensity trajectory, such as that shown in Figure 3*D* for diI in PMMA. From the coarse-time view, one can get a sense of the frequency of ISC at this excitation intensity, and in the expanded view, one can see the duration of the dark periods. A histogram of the dark period duration is presented in Figure 3*E*. A single exponential fit to the data gives the T_1 lifetime (1 ms) directly. The $S_1 \rightarrow T_1$ branching ratio can be determined by the average number of photons emitted during the "on" state. One method for determining the branching ratio is to generate histograms of the number of photons emitted per unit time, such as that in Figure 3*F*, for various time bins. In the solution phase, the triplet lifetime is significantly shorter because of the higher mobility of the triplet quenchers. As the excitation rate is lowered from the saturation level, the amplitude of intensity fluctuation reduces and eventually vanishes. In addition to trapping in the triplet state, there are other mechanisms for single-molecule intensity fluctuations, as is discussed below.

At room temperature, relaxation from the triplet to the ground state is radiationless, as is the case for internal conversion from the singlet excited state to the ground state. The energy released from these radiationless transitions causes a transient heating of the molecule and its local environment. In condensed media, the intramolecular modes and the relevant intermolecular modes are sufficiently well coupled to a high density-of-states bath so that complete vibrational relaxation occurs before the molecule can be excited again. The amount of the energy released through the repeated radiationless relaxation, in addition to that released in each excitation-emission cycle because of the Stoke's relaxation, is insufficient to create a noticeable increase in the bulk temperature of the sample. It may, and frequently does, result in photoinduced spectral jumps (discussed below).

The long-lived triplet state is implicated in photobleaching through two different mechanisms. The first is photooxidation (35, 36). Triplet organic molecules react with ground-state molecular oxygen in a triplet-triplet annihilation process,

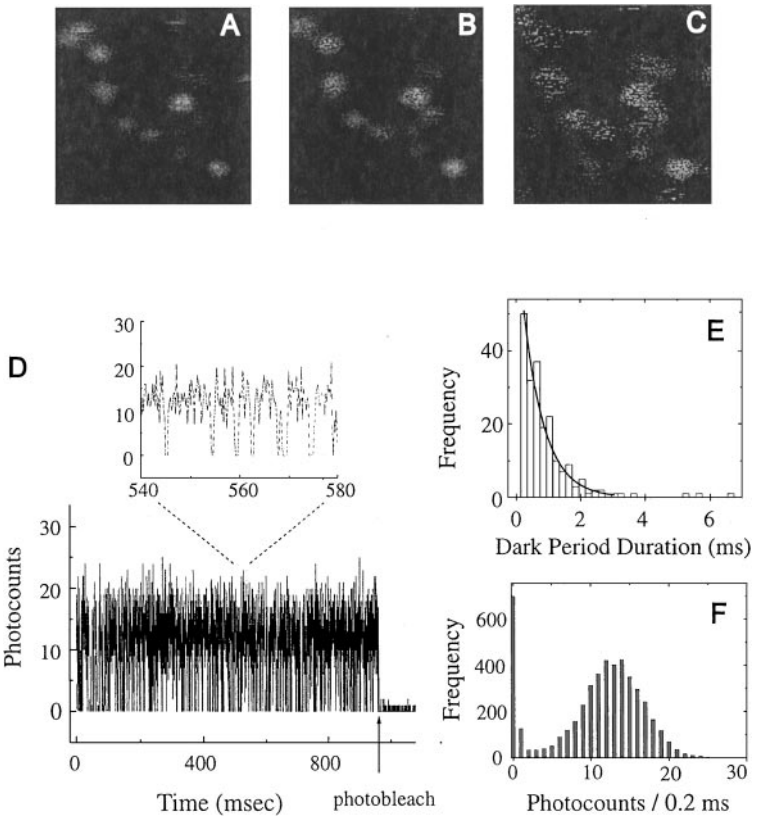

Figure 3 Images of a group of single molecules obtained at constant excitation energy. The excitation power and pixel acquisition time were (*A*) 0.3 μW and 10 ms, (*B*) 4.3 μW and 1.0 ms, and (*C*) 33 μW and 0.1 ms. The pocked appearance of the fluorescence images at the higher scan rates is due to the molecule having undergone a quantum jump into a dark state, then a jump back to the light state. (*D*) Fluorescence emission intensity versus time. (*D, upper*) The duration of the dark periods can be distinguished. (*E*) Occurrence of dark periods of a given duration. The exponential fit yields the T_1 lifetime (1 ms). (*F*) Occurrence of a given number of counts per unit time from which the $S_1 \rightarrow T_1$ branching ratio can be determined. [Reprinted with permission (33).]

yielding excited singlet oxygen and the ground-state organic molecule. The organic molecule may then be irreversibly oxidized by the singlet oxygen. The average period during which a molecule can be repetitively photo-excited prior to photobleaching is inversely proportional to excitation intensity and dependent on the local environment. For example, oxygen diffuses more slowly in a PMMA film than in a fluid solution, significantly reducing the rate of photobleaching. Figure 4*A* is the histogram of the total number of photons emitted

by individual sulforhodamine 101 molecules in PMMA before photobleaching. The fit is multiexponential, indicative of an inhomogeneous distribution of environments.

The second mechanism for photobleaching applies to the high end of the range of excitation powers typically used in single-molecule experiments where nonlinear photochemical pathways can become important. One relaxation channel from an excited state is through the absorption of an additional photon.

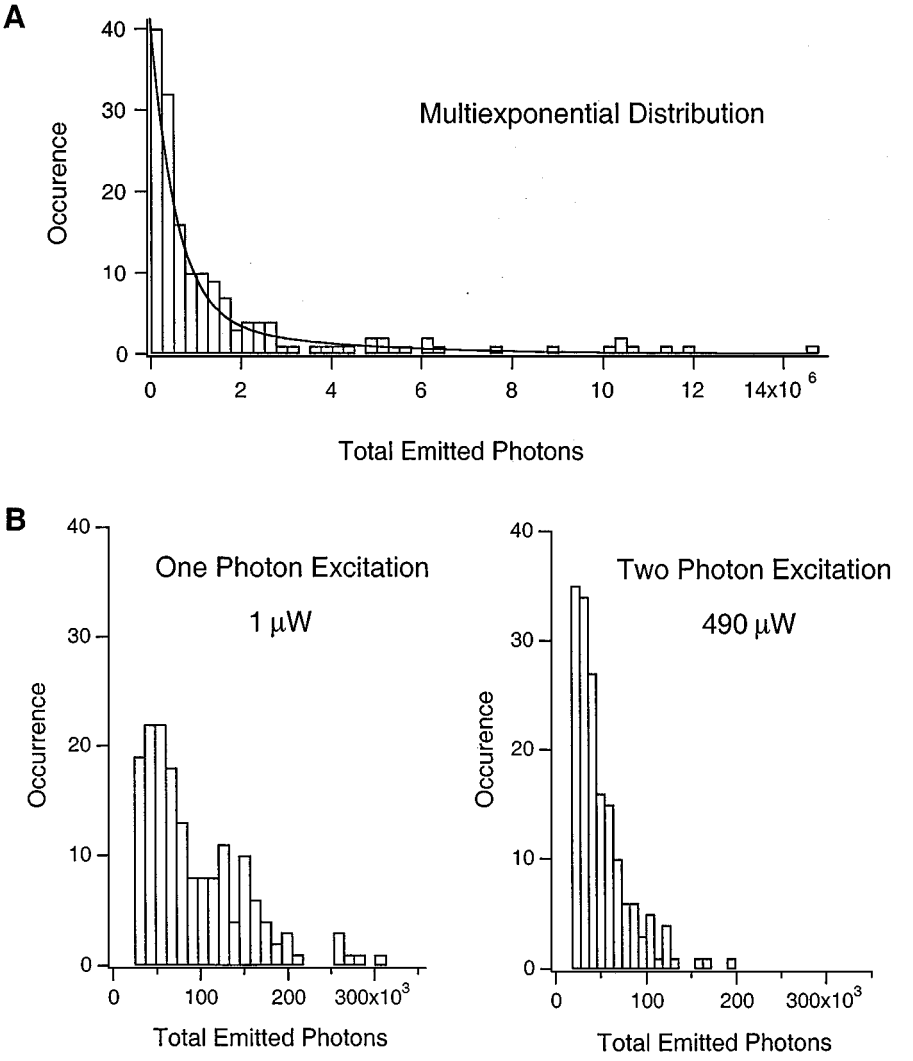

For simplicity, assume that the excited-state absorption cross-sections for the $S_1 \rightarrow S_N$ and $T_1 \rightarrow T_N$ transitions are of the same magnitude, and that the probabilities of a photochemical reaction from the doubly excited states are also roughly equivalent. Then, because the T_1 lifetime is substantially longer than the S_1 lifetime, multiphoton photochemistry proceeds predominantly through the triplet manifold. Triplet-triplet absorption—which results in a highly reactive excited state from which irreversible chemical reactions, such as hydrogen abstraction, can occur—has been extensively studied in the developments of laser dyes (37). Recently, this process has been evidenced in single-molecule experiments with two-photon excitation (24, 38). Figure 4*B* shows the comparison of photobleaching lifetimes of single rhodamine B molecules on a glass surface for one-photon and two-photon excitation. The higher average power used in the two-photon excitation results in fewer total emitted photons before photobleaching. Although the term photobleaching is used nearly synonymously with the term photochemical reaction, an interesting example of a photochemical transformation of one fluorophore into another has been reported by Shear et al (39). In a three-photon microscopy experiment, the authors discovered a reaction of four-photon-excited seratonin molecules resulting in chromophores that emitted in the green spectral region, in contrast to the UV-emitting seratonin. Similarly fortuitous photochemistry will likely be discovered in future single-molecule experiments.

Purging oxygen from the sample usually enhances fluorophore photostability. Some fluorophores, such as green fluorescence protein (GFP), are amazingly photostable even in aerobic conditions (40), presumably due to protection of the chromophore by the protein environment. GFP was developed as a noninvasive in situ fluorescent marker for cellular imaging (41). Two groups have made the

←

Figure 4 (*A*) Histogram of total emitted photons before photobleaching for 163 individual sulforhodamine 101 molecules in polymethylmethacrylate (PMMA) film. The distribution is fitted with a double exponential (*solid line*) with photobleaching lifetimes of 5.6×10^5 and 3.1×10^6 photons and weights of 89% and 11%, respectively. The molecules were excited by 0.5 μW of 532-nm laser light focused with an NA 1.4 objective lens. Both lifetimes are found to be inversely proportional to excitation intensity. The emission collection efficiency of the detection system was 10%. (Courtesy of L Ying, Pacific Northwest National Laboratory.) (*B*) Comparison of the photobleaching lifetimes for one-photon (*left*) and two-photon (*right*) excitation of single rhodamine B molecules on a glass surface, with 1 μW of 532-nm continuous wave laser light used for the one-photon excitation (to S_1 state). A femtosecond pulse train (840 nm, 120-fs pulse width, 76-MHz repetition rate, and 490-μW average power) was used for the two-photon excitation (to the second excited state, S_2). The average numbers of photons emitted from the S_1 state before photobleaching are 9.2×10^4 and 5×10^4 for the one- and two-photon excitation, respectively. The significantly shorter photobleaching lifetime for the two-photon excitation is due to the higher average power used, which results in photodamage via triplet-triplet absorption: $S_0 \overset{hv}{\rightarrow} S_2 \rightarrow S_1 \rightarrow T_1 \overset{hv}{\rightarrow} T_n \rightarrow$ H abstraction. [Reprinted with permission (24).]

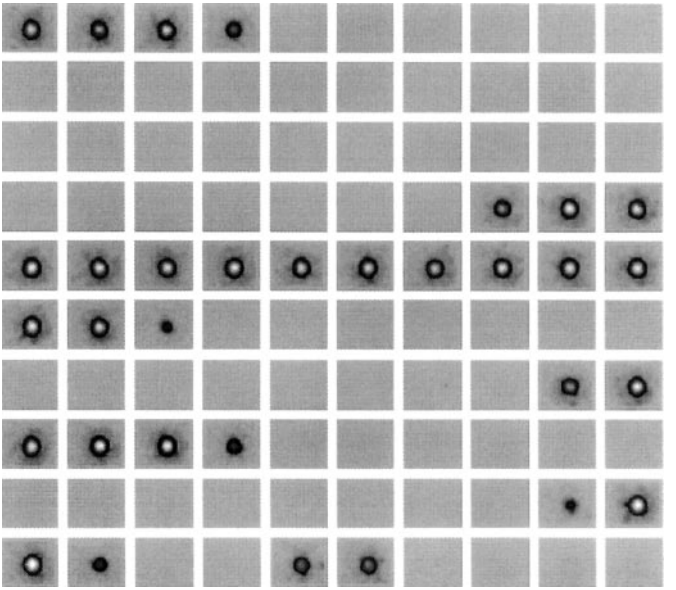

Figure 5 A sequence of 100 images of the emission from a single green fluorescence protein mutant molecule embedded in polyacrylamide gel. Each frame was taken with 100-ms exposure to a 488-nm laser excitation in a total-internal-reflection geometry. The blinking behavior is dependent on excitation intensity. [Reprinted with permission from *Science* 277:1059 (1997). See Reference 40 for details.]

interesting observation that the emission of a single GFP molecule blinks on and off on the second timescale when exciting with 488-nm light (40, 40a). Figure 5 shows a sequence of images of a blinking single GFP. Similar but less frequent blinking behavior has also been seen for some but not all single choromophores (42). A general strategy to distinguish photoinduced and spontaneous processes is to check the excitation intensity dependence. This approach appears many times throughout this chapter. Using this approach, Dickson et al found that the blinking is due to a photo-induced chemical process for the mutants of GFP examined (40). The chemical nature of the photoproducts associated with the blinking behavior has yet to be resolved for GFP and other molecules. Moreover, after emission of 10^6 photons, the GFP mutant molecules end up in a long-lived dark state, presumably the neutral form of GFP, which can be optically switched back to the original anion form by illumination with light at a different wavelength (405 nm) (40). This is another interesting example of photochemical transformation.

SPECTRAL FLUCTUATIONS

Interestingly, emission spectra of single dye molecules were found to change with time at room temperature (16). Similarly, the emission intensities of single molecules fluctuate as the result of the spectral changes (17, 42). These intrinsic fluctuations contain rich dynamic information of single molecules and their interacting environments. Lu & Xie have carried out a detailed study of the origins for the spectral fluctuations (43).

Figure 6*A* shows a sequence of emission spectra for a sulforhodamine 101 molecule in PMMA taken at room temperature (170-ms collection time per spectrum). Significant variations in the spectra are evident. The simultaneous trajectories of the spectral mean and the emission intensity (integrated area under each spectrum) for another molecule are shown in Figures 6*B* and *C*, respectively. The data were taken at an excitation rate well below saturation; therefore, the intensity fluctuations were not due to ISC to the triplet state, as discussed earlier. An anticorrelation between the spectral trajectory and the intensity trajectory is evident: A blue-shifted emission (and absorption) spectrum results in a decrease in emission because of a smaller absorption at the excitation wavelength (594 nm), which is at the red edge of the absorption band. The cross-correlation function of the spectral mean and the intensity [$\langle \Delta\bar{\omega}(0)\Delta I(t)\rangle$, Figure 6*D*] decays on the same timescale as the autocorrelation functions of the intensity [$\langle \Delta I(0)\Delta I(t)\rangle$, Figure 6*E*] and the spectral mean [$\langle \Delta\bar{\omega}(0)\Delta\bar{\omega}(t)\rangle$, not shown], further proving the anticorrelated relationship. Similarly, a correlated relationship was observed for an excitation wavelength (532 nm) at the blue edge of the absorption band. Because translational or rotational diffusion motion, if any, is infrequent in this system, the spectral fluctuation was attributed to variations of either the intermolecular nuclear coordinates (such as hydrogen bonds or collective motion of the surrounding molecules) or intramolecular nuclear coordinates (the conformation of the chromophore).

It is instructive to review the spectral hole-burning work done at cryogenic temperature (44). In a conventional spectral hole-burning experiment, a subset of molecular transitions in an inhomogeneously broadened ensemble is selectively excited with a narrow laser line, and the transition frequencies of the subset are shifted, resulting in a narrow hole in the absorption band. Nonphotochemical hole-burning (45) denotes access to a different potential minimum in the ground electronic state (thus, a transition frequency shift) through photoexcitation to and relaxation from the singlet excited state. The spectral hole is broadened and filled with time as the result of spectral diffusion, i.e. molecules undergoing spontaneous changes on the ground state potential surface (46). At room temperature, the homogeneous linewidths become comparable to the inhomogeneous width. Spectral hole-burning under this condition is difficult, if

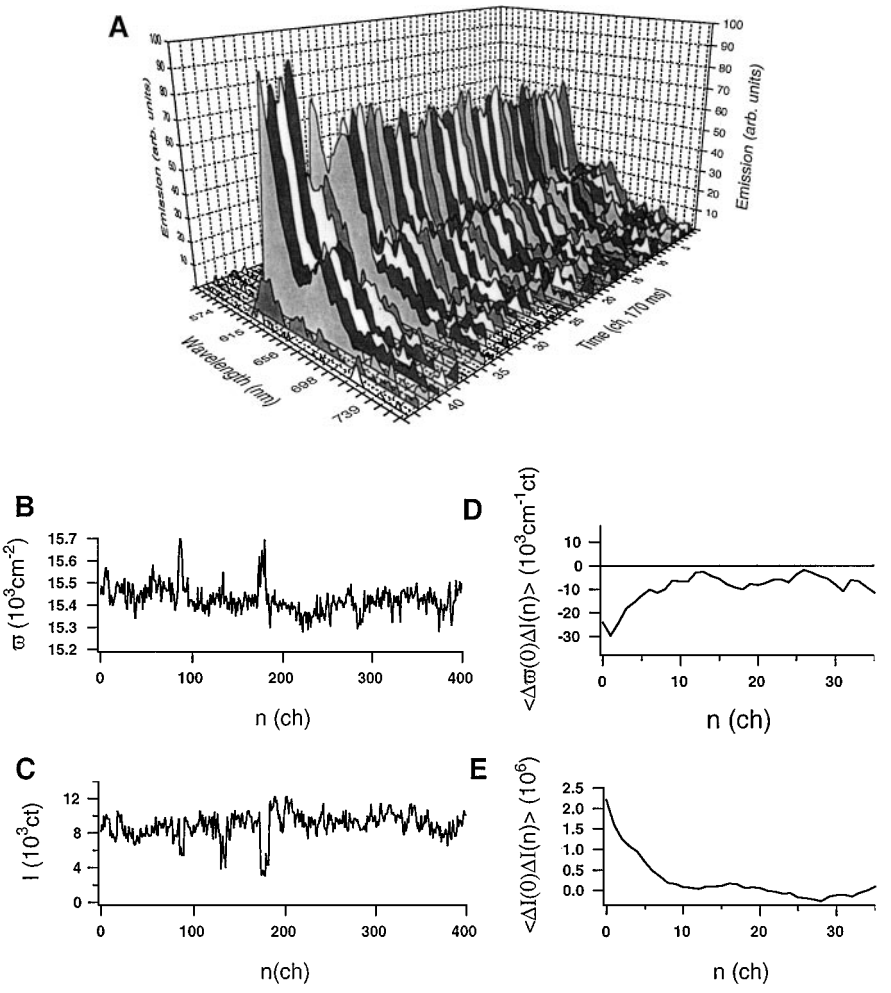

Figure 6 (*A*) Emission spectra of a single sulforhodamine 101 molecule on polymethylmethacrylate taken sequentially with 170-ms data collection times. Significant spectral shifts are observed (see 43 for details). (*B*) Trajectory of the spectral mean ($\bar{\omega}$) of another molecule excited at 594 nm, the red edge of the absorption spectrum. *n* is the index number of the spectra. (*C*) Simultaneous trajectory of the total emission intensity (*I*, integrated area of each spectrum) of the molecule. (*D*) Cross correlation function of $\bar{\omega}$ and *I*, $\langle \Delta\bar{\omega}(0)\Delta I(n)\rangle$, clearly showing an anticorrelated relationship between $\bar{\omega}$ and *I*. A correlated relationship was seen for excitation at the blue edge of the absorption spectrum. (*E*) Autocorrelation function of *I*, $\langle \Delta I(0)\Delta I(n)\rangle$, which decays with the same rate of $\langle \Delta\bar{\omega}(0)\Delta I(n)\rangle$. (Courtesy of HP Lu, Pacific Northwest National Laboratory.)

not impossible. Single-molecule spectral trajectories provide a unique window to spectral dynamics in condensed-phase systems. Both spontaneous spectral fluctuations (spectral diffusion) (47) and photoinduced spectral fluctuations (nonphotochemical hole-burning) (48) have been observed on individual molecules at cryogenic temperature. Compared with the low-temperature spectral fluctuations, the fluctuation in Figure 6 has a much larger amplitude, indicating the significantly different energy landscape probed and the microscopic mechanisms involved at room temperature. As discussed by Myers in this volume (49), spectral dynamics on the sub-picosecond timescale result in broad electronic line shapes at room temperature. It is intriguing that the room-temperature spectral fluctuations observed in the single-molecule measurement occur on very long timescales.

Figure 7*A* shows a typical autocorrelation function of the spectral mean at room temperature, which was fitted with a double exponential decay, with the faster rate $k_1 = 2\ s^{-1}$ and the slower rate $k_2 = 0.02\ s^{-1}$. The double exponential behavior of $C(t)$ led to the conclusion that there have to be two quasi-independent types of nuclear motions taking place with two different rates. k_1 was found to be independent of the excitation rate, indicating that the faster fluctuation is spontaneous spectral diffusion. This was further confirmed by a shuttering scheme (Figure 7*B*, *inset*) in which excitation light is periodically blocked for a waiting time after each spectrum collection. Figure 7*B* shows the spectral autocorrelation function of the same molecule, $C(n)$, with n the index number of the spectra. If the spectral fluctuation were photoinduced, Figure 7*A* would be identical to Figure 7*B*. The disappearance of the faster decay component in Figure 7*B* indicates that significant spectral diffusion occurs during the waiting time. In contrast to k_1, k_2 was found to have a linear dependence on the excitation rate, indicating that the slower fluctuation is primarily photoinduced. The photoinduced fluctuations originate from either nonphotochemical hole-burning or radiationless transitions. The slow rate is associated with the low quantum yield ($\leq 10^{-6}$) for either of the mechanisms. Dominated by the photoinduced processes ($k_{2\text{phto}}$), k_2 also has a contribution from spontaneous fluctuations, $k_{2\text{ther}} = k_2 - k_{2\text{phto}}$, which can be determined by the shuttering scheme (43). Both spectral diffusions (k_1 and $k_{2\text{ther}}$) have been otherwise hidden in ensemble-averaged experiments.

The distinct difference between k_1 and $k_{2\text{ther}}$ indicated that there are two types of barrier heights in the multidimensional potential energy surface of the molecule (Figure 7*C*): k_1 and $k_{2\text{ther}}$ are associated with the thermally activated transitions between the local minima and the gross minima, respectively. $k_{2\text{ther}}$ is so slow that it is often dominated by $k_{2\text{pho}}$ through photoexcitation. k_2 is anticipated to be associated with an intramolecular nuclear coordinate, whereas k_1 can be associated with either an inter- or an intramolecular

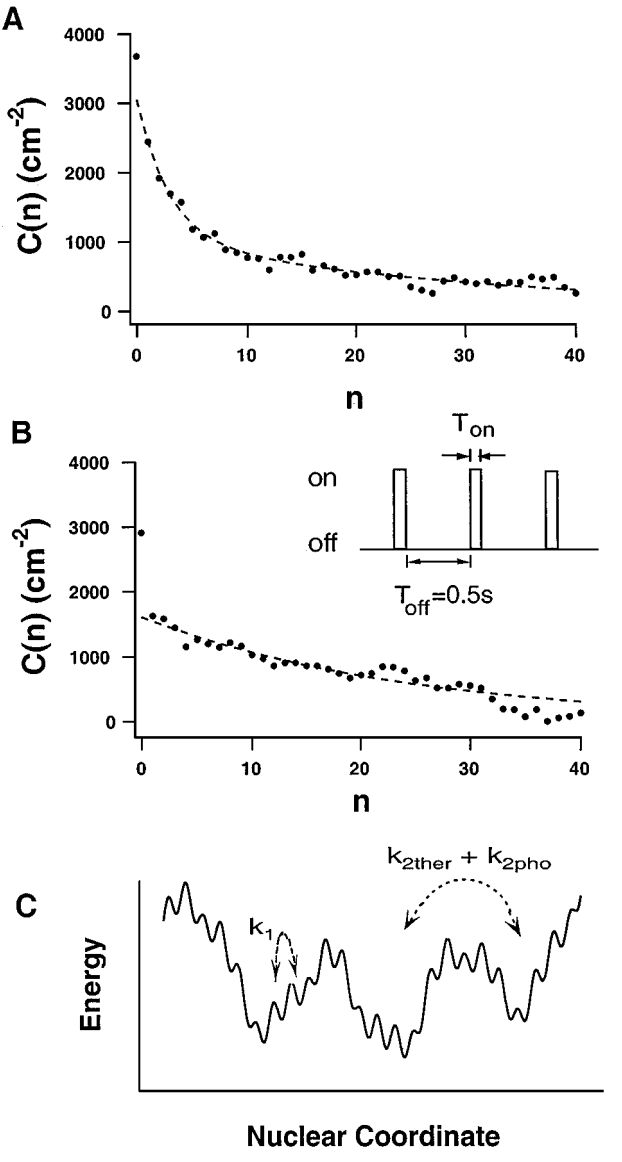
A
C(n) (cm-2)
4000
3000
2000
1000
0
0
10
20
30
40
n
B
C(n) (cm-2)
Ton
on
off
Toff=0.5s
n
C
Energy
k1
k2ther + k2pho
Nuclear Coordinate

coordinate. The single-molecule experiment has allowed the probing of the potential energy surface in a particular environment. Potential energy surfaces with such multiminima have been proposed for proteins (50). Similar experiments hold promise for probing conformational motions and energy landscapes of proteins.

SINGLE-MOLECULE RAMAN SPECTROSCOPY

Single-molecule spectroscopy has produced a number of interesting discoveries. No result has been more surprising or controversial than two reports that appeared in early 1997 (25, 26) claiming the detection of surface-enhanced Raman scattering from single molecules. Figure 8 shows a sequence of such Raman spectra with an impressive signal-to-noise ratio. The gradual decrease of the total intensity has yet to be explained. More than 20 years have passed since the first report of enhanced Raman scattering from a molecule situated on a roughened silver surface (51, 52). The attention of researchers to the effect resulted in hundreds of papers. Although the experiments varied, the increase in Raman scattering for a molecule on a colloidal or roughened silver surface was generally accepted to be as large as $\sim 10^6$. The recent single-molecule experiments put the enhancement factor several orders of magnitude higher.

Whether Raman scattering from one molecule has been observed or not is probably less important than the undeniable fact that both Nie & Emory (25) and Kneipp et al (26) found surprisingly large Raman scattering cross-sections, which is not only fascinating but possibly useful. As both groups point out, the advantages of Raman over fluorescence are that it is vibrationally resolved, even at room temperature, and photochemical bleaching is diminished. Both of these

←

Figure 7 (*A*) Autocorrelation function $C(n) = \langle \bar{\omega}(0)\bar{\omega}(\mathrm{n})\rangle$, for a single sulforhodamine 101 molecule on polymethylmethacrylate under 594-nm excitation, *n* being the index number of spectra (continuously taken with T = 170-ms collection time). (*dashed line*) A double exponential fit, $C(n) = a_1 \exp(-k_1 nT) + a_2 \exp(-k_2 nT)$, with a fast component ($k_1 = 2.1\ \mathrm{s}^{-1}$) and a slow component ($k_2 = 0.02\ \mathrm{s}^{-1}$). The fast component is shown to be due to spontaneous fluctuation, whereas the slow component has both photoinduced ($k_{2\mathrm{pho}}$) and thermal ($k_{2\mathrm{ther}} = k_2$–$k_{2\mathrm{pho}}$) contributions. (*B*) A stuttering scheme (*inset*) in which the excitation light is periodically blocked for a dark time ($T_{\mathrm{off}} = 500$ ms) after each spectral collection time ($T_{\mathrm{on}} = 170$ ms). (*dotted line*) $C(n)$ for the same molecule in *A*. The fast component disappears, proving it is indeed associated with spontaneous fluctuation during *T*. (*dashed line*) A single exponential fit, $C(n) = a_2 \exp[-\mathrm{n}(k_2 T_{\mathrm{on}} + k_{2\mathrm{ther}} T_{\mathrm{off}})]$, yielding $k_{2\mathrm{ther}} = 0.02\ \mathrm{s}^{-1}$. (*C*) A schematic of the potential energy surface of the nuclear coordinates. At least two distinctly different types of barrier heights exist. The fast thermal fluctuation (k_1) is associated with crossing the small barriers, whereas photoinduced ($k_{2\mathrm{pho}}$) and slow thermal ($k_{2\mathrm{ther}}$) fluctuations are associated with crossing the large gross barriers. [Reprinted with permission (43).]

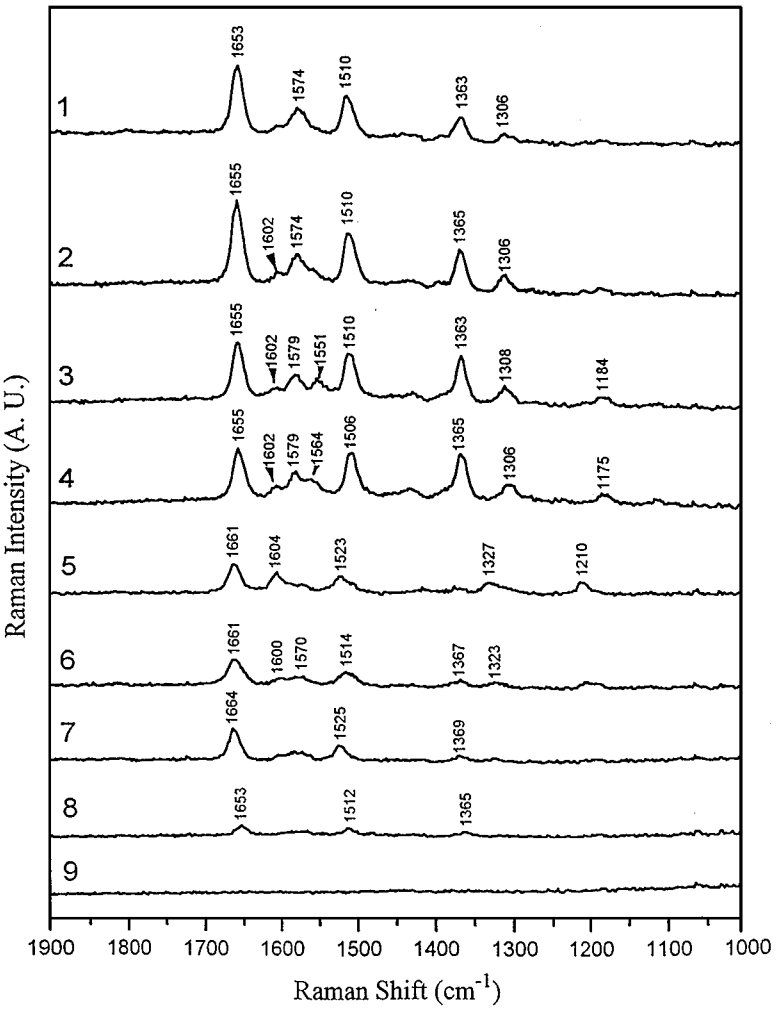

Figure 8 Surface-enhanced and resonance-enhanced Raman spectra of a single R6G molecule on a Ag particle recorded at 1-s intervals. More than 300 spectra were recorded from the particular Ag particle before the signals disappeared. Nine spectra were selected to show sudden spectral changes. Abrupt changes in both frequency and intensity are seen in spectra 2, 5, and 8. The R6G concentration was 2×10^{-11} M, corresponding to an average of 0.1 molecule per particle. Laser wavelength, 514.5 nm; laser power, 10 μW; and focus radius, $\sim$250 nm. [Reprinted with permission (25).]

aspects are important in fundamental and applied studies using single-molecule spectroscopy.

It is generally accepted that two effects contribute to the enhancement of surface-enhanced Raman scattering. These are referred to as chemical enhancement and field enhancement. The 1985 review by Moscovits (51) focused on field enhancement. Calculations and experiments were presented to explain the $\sim 10^6$ increase in the scattering cross-section. Chemical enhancement (52) was recognized as contributing in certain instances, but that contribution was characterized as never amounting to more than a factor of 10. At about the same time, Hildebrandt & Stockburger (53) published a paper demonstrating convincingly that there are two types of binding sites on colloidal-Ag particles prepared (54) and subsequently activated with various anions. Importantly, the more stable site occurs at low number, a few per particle, and molecules chemisorbed at those sites show enhanced Raman scattering nearly three orders of magnitude greater than the molecules nonspecifically adsorbed to the surface. The experiments of both Nie & Emory (25) and Kneipp et al (26) use similarly prepared colloids at dye-to-colloidal particle concentrations where only the more stable, more highly enhanced sites are populated.

The experimental procedure of Nie & Emory (25) consisted of dispersing colloidal particles, which had been incubated with dye, onto a substrate. This enabled protracted interrogation of individual colloidal particles. The dye-particle concentration was 1:10, on average. One would expect a result consistent with that of Hildebrandt & Stockburger (53), given the preparation of the colloid, the low dye-particle concentration, and the choice of excitation wavelength resonant with the molecular absorption. The latter reported a surface enhancement of 10^6 in the presence of the colloid. (The authors did not characterize the total scattering cross-section but the enhancement over non–surface-enhanced resonant Raman scattering. Another factor of 10^5 enhancement is typically expected when on resonance with a molecular electronic transition, resulting in a likely total enhancement over nonresonant and non–surface-enhanced Raman of $\sim 10^{10}$–10^{11}.) Instead, Nie & Emory observed a very few, very bright particles. In rough numbers, they reported that 1 in $\sim 10^3$ particles exhibited detectable Raman emission, but that the enhancement over nonresonant and non–surface-enhanced Raman for those bright particles was $\sim 10^{14}$ (25).

The average size of colloidal particles was $\sim$35 nm, and at the concentration of activating anions used ($\sim$1 mM NaCl), the particles were not significantly aggregated. Yet when the so-called hot particles were examined with an atomic force microscope, the average size was found to be 100 nm. The authors hypothesize that only those particles resonant with the excitation wavelength are observed in the experiment. If this hypothesis holds, it will prove to be one of

the more dramatic examples of selection from an inhomogeneous population in single-entity spectroscopy. The evidence that scattering originated from single molecules is the 1:10 dye-particle ratio, some spectral wandering (Figure 8), and polarized emission. None of these constitutes proof. The full analysis of these issues requires further experimentation.

There are two important differences between the experiments of Nie & Emory (25) and Kneipp et al (26): Kneipp et al used a Cl concentration approximately 10 times higher than that used by Nie & Emory, resulting in a higher degree of aggregation of the individual colloidal particles; and the excitation wavelength was in the near-infrared (∼830 nm). The results are even more striking than those of Nie & Emory in that essentially every molecule was observed. In addition, the excitation was off both the molecular resonance and the principal particle resonance. The sample was not deposited on a substrate but examined in solution, in which the counting of emitting species supported the claim of scattering from a single molecule. The dye-particle ratio was 1:100. Thus, hot-particle selection could be operative, but only if the resonant particles also have the preferential binding sites.

Many questions about the nature of the resonances remain to be answered. But interest has been stimulated, and surface-enhanced Raman will likely be one of the more active areas of research in the coming years.

DIFFUSIONAL MOTIONS

Molecular diffusion in different systems has been a subject of extensive studies. Single-molecule diffusional trajectories can now be directly recorded. Figure 9*A* shows the translational diffusion trajectories of individual fluorescence-labeled lipid molecules in a fluid lipid membrane, recorded by Schmidt and coworkers using a CCD camera (21). The accuracy of determining the center positions of diffraction-limited fluorescence spots can be as high as a few nanometers. Statistical analysis of the trajectories was carried out to evaluate the mean-square-displacement (MSD) as a function of time lags: MSD $(t_{\text{lag}}) = 4D_{\text{lat}}\, t_{\text{lag}}$ (Figure 9*B*). A particularly interesting finding was that the D_{lat} is time dependent (Figure 9*C*). This was interpreted as the result of island structure of the membrane surrounded by barriers for lipid diffusion. The usefulness of similar experiments on membrane transport of biological systems cannot be underestimated. The diffusion trajectories of single dye molecules in a polymer matrix have also been recorded with near-field microscopy (55, 56), in polyacrylamide gels (22), and in solution with CCD cameras (57).

For solution-phase measurements with a fixed laser focus, a single molecule can diffuse in and out of the excitation volume, which—among other origins—results in intensity fluctuations (13, 58, 59). A particularly useful approach in

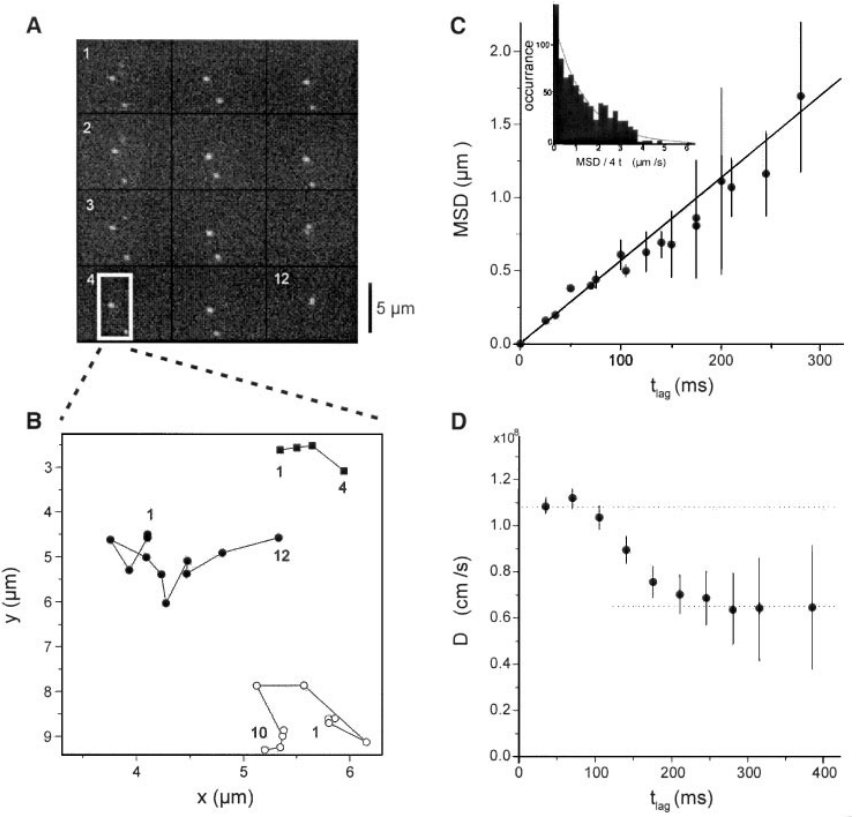

Figure 9 (*A*) Twelve sequential images of a 12.2 × 9.5 μm^2 area of a fluid lipid membrane containing three fluorescently labeled lipid molecules. Supported lipid bilayer of 1-palmitoyl-2-oleoyl-sn-glycero-3-phosphocholin are transferred onto a glass substrate by the Langmuir-Blodgett technique. Fluorescent analogues of 1-palmitoyl-2-oleoyl-sn-glycero-3-phosphoethanolamine are labeled with tetramethylrhodamine. Each image frame was recorded in 10 ms with a laser intensity of (57 ± 14) kW/cm^2. (*B*) Translational trajectories of the three labeled molecules in *A*. (*C*) Mean square displacement (MSD) as a function of time lag, t_{lag}, obtained from 531 single-molecule trajectories. The linear fit to MSD(t_{lag}) = $4D_{lat}$ t_{lag} results in a diffusional constant D_{lat} = (1.42 ± 0.23) × 10^{-8} cm^2/s. (*inset*) Histogram of MSD/4 t_{lag} from single molecule trajectories. The exponential distribution (*solid line*) has a first moment, D_{lat} = (1.4 ± 0.3) × 10^{-8} cm^2/s. (*D*) Dependence of lateral diffusion constant (D_{lat}) as a function of time lag (t_{lag}). The variation of D_{lat} is due to the inhomogeneous lipid membrane, which results in a faster diffusion in a short time within island structures in the membrane and in a slower diffusion over a long time between islands. The average size of the islands is ∼400 nm. [Reprinted with permission (21).]

analysis of such an intensity fluctuation is fluorescence correlation spectroscopy (FCS) (60, 61), a technique first developed in the 1970s for studying concentration fluctuations of chemical reactions (62). In FCS, an intensity autocorrelator is used to measure and signal average the intensity autocorrelation function in real time. The technique was recently advanced to single-molecule sensitivity (13, 23). One notes, however, that a typical FCS trace is the result of a large number of individual molecules diffusing one at a time in and out of the focal volume. Occurring on different timescales, triplet trapping and translational diffusion are reflected in an FCS trace, as are other dynamical processes such as conformational or chemical changes (see below). A noteworthy recent finding is that a focused laser beam can generate a trapping potential for sizable molecules, which can alter the statistics of intensity fluctuations (63).

The ability to determine single-molecule orientations allows the observation of rotational motion of single molecules. By using a polarization modulation scheme, Ha et al directly observed rotational jumps of single fluorophores on a surface (42). Recently, they developed a more sophisticated scheme to monitor free and hindered rotation (64). As shown in Figure 10*A*, the polarization direction (θ) of the excitation light is rotated in time. After passing through a polarization beam splitter, emission in the $\hat{s}$ and $\hat{p}$ polarization directions are recorded with time. A fixed dipole ($\Delta\phi_{max} = 0$) results in sinusoidal modulations in both directions with no phase difference. Assuming the rotational correlation time is longer than the fluorescence lifetime, a freely rotating dipole ($\Delta\phi_{max} = 90^\circ$) results in a reduction in the modulation depths and a 180° phase difference between $\hat{s}$ and $\hat{p}$ directions. In general, hindered rotation diffusion within a cone angle ($\Delta\phi_{max} \neq 0$) results in a certain phase shift between the $\hat{s}$ and $\hat{p}$ directions. The technique was used to study a Texas Red fluorophore covalently tethered to a short DNA molecule by a flexible carbon chain

Figure 10 (*A*) Experimental arrangement: Excitation field *E*, with an angle of θ relative to $\hat{p}$, is rotating with time; *z* is the propagation direction for the exciting field; $\vec{\mu}_a$ and $\vec{\mu}_e$ are the molecular dipole moments for absorption and emission. The dipole moment is constrained to a cone with a center angle ϕ_0 and a half cone angle $\Delta\phi_{max}$. The emission collected along $\hat{z}$ is split by the polarizing beam splitter and the two signals, I_s and I_p, are simultaneously recorded. (*inset*) A DNA molecule bound to a glass surface with a tetramethylrhodamine (TMR) label covalently bound to the end of the DNA. (*B*) The simultaneous I_s and I_p of a single TMR label. (*C*) The cycle-averages of the trajectories in *B*. The 180° phase difference between $\hat{s}$ and $\hat{p}$ indicates an almost freely rotating molecule. (*D*) Cycle-averaged I_s and I_p for another fluorophore. The zero phase difference indicates a fixed dipole of the TMR. (*E*) ϕ_o (*gray line*) and $\Delta\phi_{max}$ (*black line*) trajectories of a TMR label. The TMR label jumps above the surface and freely spins before landing back on the surface with the original orientation. The frequency of the rotational jump is found to be linear with respect to the excitation power, indicating a photoinduced process. [Reprinted with permission (64).]

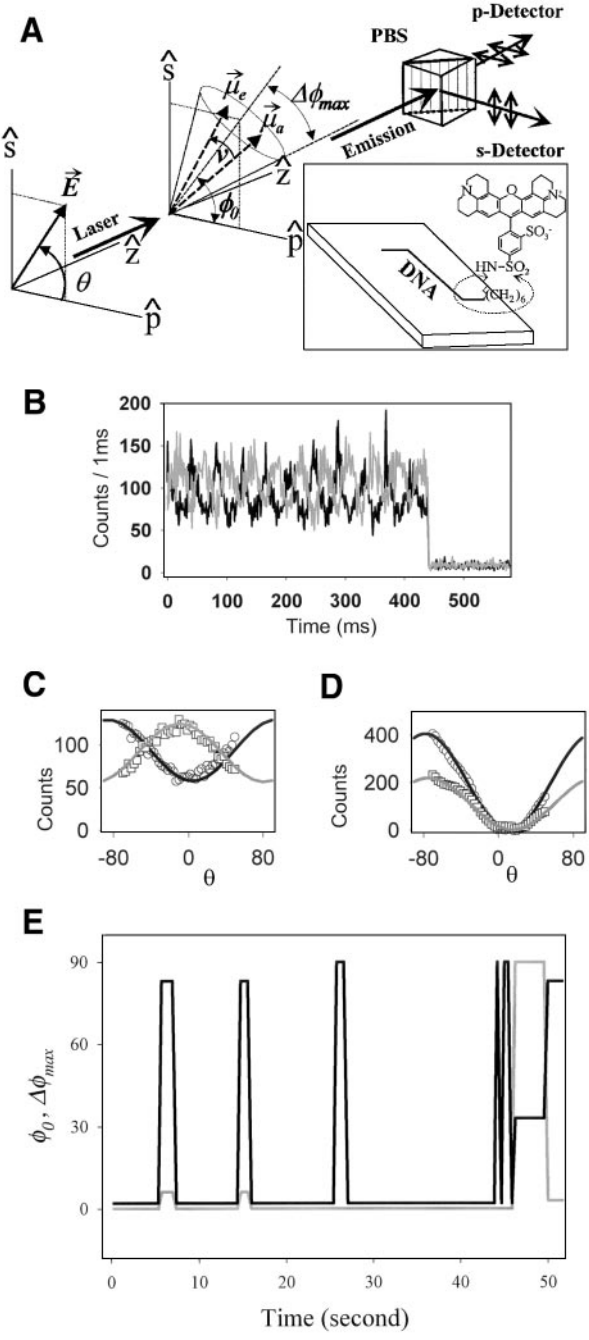
A
p-Detector
PBS
s-Detector
Emission
Laser
DNA
B
Counts / 1ms
Time (ms)
C
Counts
θ
D
Counts
θ
E
ϕ_0, $\Delta\phi_{max}$
Time (second)

(Figure 10*A*, *inset*). The DNA is adsorbed onto a glass surface under a buffer solution. Figure 10*B* shows $\hat{s}$ and $\hat{p}$ traces of a single fluorophore that undergoes nearly free rotation in solution, with the cycle average shown in Figure 10*C*. Figure 10*D* shows the cycle average of another fluorophore with a fixed dipole on the surface or the DNA. An intriguing observation was made that some fluorophores undergo a rotational jump above the surface, then proceed with hindered rotational diffusion in the solution phase before landing on the surface again. Figure 10*E* shows trajectories of ϕ_0 and $\Delta\phi_{\max}$ for such a fluorophore. The intensity dependence of the jumping frequency proved that the rotational jumps are photoinduced rather than spontaneous. Interestingly, the fluorophore repeatedly reabsorbed to the same orientation (ϕ_0), indicating a favorable binding site to the DNA or the surface. The promise of this technique lies in its ability to monitor conformational motions for immobilized macromolecules.

CONFORMATIONAL MOTIONS OF MACROMOLECULES

The emission lifetime of a fluorescent label in a macromolecule, when dominated by nonradiative relaxation, is sensitive to the local environment and can serve as a good probe for conformational motions of the macromolecule. Edman et al (65, 65a) studied lifetimes of a tetramethylrhodamine (TMR) fluorophore attached with a six-carbon linker to an 18-mer DNA sequencing primer in solution (Figure 11). The ensemble-averaged result shows a double exponential decay with time constants of 0.86 and 3.70 ns with equal amplitudes. On a single-molecule basis, the measured fluorescence decays are also double exponential, but the amplitudes vary from 0 to 1 from molecule to molecule. This observation indicated that there exist two conformations in a single molecule, which interconvert at a timescale comparable to that of the measurements. As shown in Figure 11, a model was proposed in which the conformation with the longer lifetime corresponds to the TMR surrounded by water molecules, whereas the conformation with the shorter lifetime corresponds to a close contact between TMR and the guanosines of the oligonucleotide. In the latter case, TMR fluorescence is quenched by the guanosines through a nonradiative pathway. Because conversions between the two conformations result in emission intensity fluctuation on a different timescale than triplet lifetime ($<$1 ms) or diffusional time ($\sim$250 ms), Edman et al were able to determine experimentally the timescale of the conversion with FCS. Assuming a stretched exponential behavior for the conversion, the relaxation time, $1/k$, was determined to be (23 ± 13) ms. In a more recent work, Rigler and coworkers were able to directly observe the conformational motion in real time by recording an emission intensity trajectory (66).

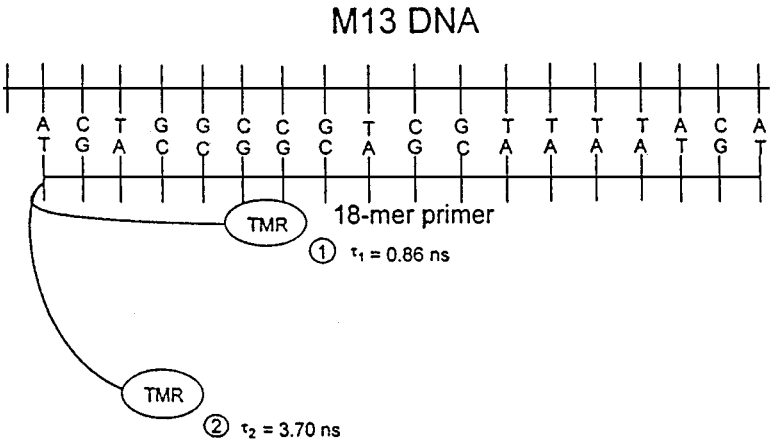

Figure 11 Model of conformational motion of a tetramethylrhodamine (TMR) fluorescent label attached with a six-carbon chain to an 18-mer DNA. The two states (*1* and *2*) have different fluorescence lifetimes. (*state 1*) TMR forms a complex with guanosine and has a shorter fluorescence lifetime. (*state 2*) There is no contact between TMR and guanosine. [Reprinted with permission (65).]

Similarly, Jia et al studied fluorescence decays of individual TMR-tRNA^{Phe} adducts immobilized on a silanized glass surface (67). The specifically labeled single TMR molecules also exhibit double exponential decays (Figure 12*A*), corresponding to two conformational states interchanging during the course of the measurements. The histograms of the short and long lifetimes are shown in Figure 12*B*. The shorter lifetime was attributed to the formation of a complex of TMR and an adjacent guanosine, G15 of the tRNA. Figure 12*C* shows the histogram of the fraction of the long component. This contains dynamical information masked in ensemble averaged experiments.

Pertinent to the above two experiments is the idea that inhomogeneity is dependent on the timescale of the dynamics. Inhomogeneity in this case represents two conformations, whereas the dynamics is characterized by k, the sum of forward and backward conversion rates. Geva & Skinner (68) worked out a stochastic theory based on a simple two-state jump model, which quantitatively accounts for the probability distribution of the fraction of the two conformations: $P(x)$, with $x = 1$ for a pure long component and $x = 0$ for a pure short component. $P(x)$ varies with the measurement time, τ. Analogous to Kubo's picture of motional narrowing in spectral line shape (69), in the limiting case of $k\tau \gg 1$, a rapid conversion results in a Gaussian-distributed $P(x)$ centered at the equilibrium fraction, whereas in the other limiting case of $k\tau \ll 1$, the $P(x)$ has split peaks around $x = 1$ and $x = 0$. The fitting of experimental

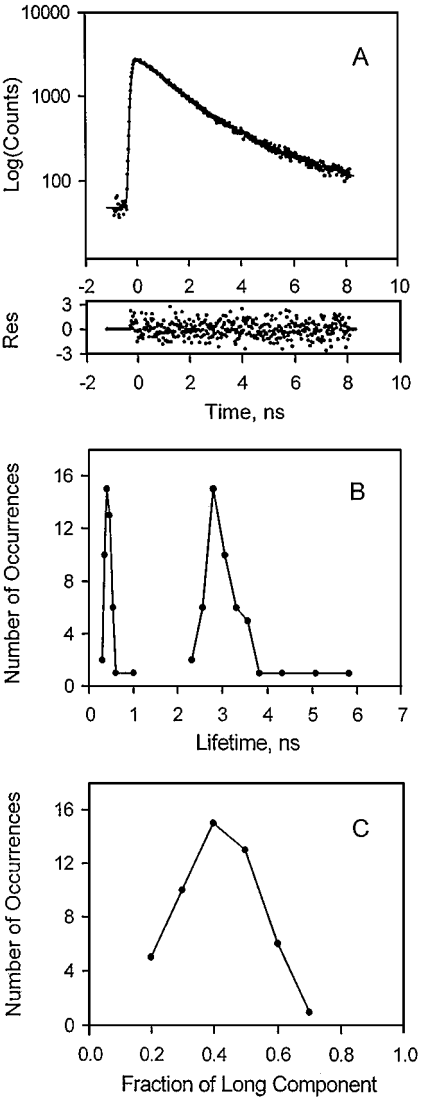

Figure 12 (*A*) Fluorescence decay of a single tetramethylrhodamine (TMR) fluorophore in a 1:1 tRNAPhe-TMR adduct, showing nonexponential decay kinetics. (*B*) Probability distribution of lifetimes. Fluorescence decays of 50 individual molecules are fitted with double exponential decays. Two distinct peaks of lifetimes are seen. (*C*) Probability distribution of the fraction of the long component. [Reprinted with permission (67).]

data by Geva & Skinner (68) yields a $k\tau$ of $\sim$5 for the system of Edman et al (65a) and a $k\tau$ of $\sim$70 for the system of Jia et al (67). The two-state model captures the essence of the conformational dynamics. Of course, all molecules in a system were assumed to be equivalent, which has neither been proved nor disproved by the experiments. As statistical analysis of further experiments improves, a stretched exponential conversion kinetics may prove to be necessary (65). This can arise from either static inhomogeneity between molecules or non-Markovian behavior (dynamical barrier change between the two conformers) within a molecule. Recent experiments also showed that more than two conformations exist in a system similar to that of Edman et al (70).

The emission spectrum and lifetime of a fluorophore in a macromolecule can probe conformational changes in the vicinity of the fluorophore. To probe conformation motions at larger scale (10–75 Å), such as folding and unfolding of proteins, fluorescence resonant energy transfer between a donor and acceptor pair can be used.

ENERGY TRANSFER

Fluorescence resonant energy transfer (FRET) has been widely used in biochemical and biophysical studies (71). In the weak interaction regime, the efficiency of FRET between a donor and acceptor pair is $E = 1/(1 + (R/R_0)^6)$, where R is the distance between the pair and R_0 is the Forster radius. R_0 is dependent on the spectral overlap between the donor emission and acceptor absorption spectra and the relative orientations of the donor and acceptor transition dipoles. FRET between single donor and acceptor pairs has been studied by Weiss and coworkers using a model system with a TMR (donor) and a Texas Red (acceptor) dye molecule attached to two ends of hybridized and complementary DNA of 10 or 20 bases (72). Dry samples of the DNA on a silanized glass surface were examined with a near-field microscope. When using 514-nm light to excite the donor preferentially, the recorded emission spectrum is normally a linear combination of the donor and acceptor spectra until photobleaching of the acceptor (or donor) results in a pure donor (or acceptor) spectrum (see Figure 13). The termination of energy transfer upon the photobleaching not only served to prove the existence of single-pair energy transfer, it also allowed the energy transfer efficiency, E, to be determined on a single-pair basis. A broad distribution of E (16–85%) was seen for individual pairs in different local environments, which was attributed to variations in distance due to the flexible six-carbon linker connecting the dye and the DNA, variations in donor and acceptor spectral overlap, and variations in donor/acceptor relative orientations. The uncertainties due to the orientation factor and spectral overlap do not permit an accurate determination of the absolute distance, R. However, it

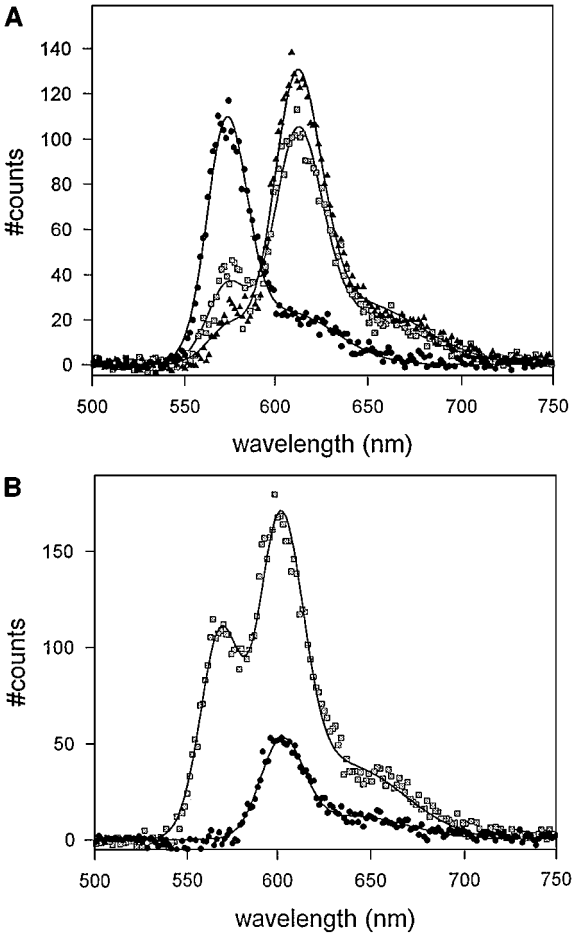

Figure 13 (*A*) Three consecutive emission spectra of a single tetramethylrhodamine (donor) and Texas Red (acceptor) pair spaced by 20 bp of DNA. (*black triangles*, *gray squares*, and *black circles*) The times sequence. Each spectrum is fit with a combination of donor and acceptor spectra (*solid lines*). Excitation at the donor gives rise to a superposition of donor and acceptor spectra (*black triangles*) due to energy transfer. Photobleaching of the acceptor (620-nm peak) results in a donor-only spectrum (*black circles*, 575-nm peak). The energy transfer efficiency (E) was determined to be 85%. (*B*) For another TMR and TR pair, the emission spectrum (*gray squares*) changes to an acceptor-only spectrum (*black circles*, 600-nm peak) upon photobleaching of the donor. E is 53% for this pair. [Reprinted with permission (72).]

is possible to use this method to monitor changes of the relative distance of a FRET pair specifically labeled in a macromolecule undergoing conformational motions. Care has to be taken to avoid complications that arise from spectral fluctuations of the labels and from librational motion of the tethered labels within the macromolecule. However, these complications might not be as serious in an aqueous environment as in a dry sample (sufficiently dry so as to restrict rotational motion) because of faster averaged motions in the former. For a given R_0, E is highly sensitive to R only in a very small range of R around R_0. An experimental challenge is to engineer a FRET pair with appropriate R_0 at the right locations to reflect motions under investigation.

When the distances between chromophores become smaller and interaction stronger, excitons are delocalized or partially delocalized in an aggregate of chromophores. Fluorescence measurements of single complexes of chromophores have been pursued by a few groups. Wu et al first reported a surprising phenomenon in B-phycoerythrin, a light-harvesting protein for photosynthesis containing a cluster of 34-bilin chromophores (73). The fluorescence intensity of a single complex undergoes a single-step photobleaching rather than the gradual disappearance expected for noninteracting chromophores. Wu et al attributed the sudden bleaching to the fact that the complex behaves as a single quantum system rather than a collection of independent chromophores. This claim was supported by the observation of photon antibunching in a photon pair correlation measurement on single complexes (73). Photon antibunching has been seen for single chromophores at cryogenic temperature (74) and room temperature (75). The essence of the phenomenon is that a single chromophore cannot emit two photons arbitrarily close in time because of the finite ground-state recovery time (a few nanoseconds); therefore, emitted photons tend to be separated from each other. Photon antibunching in the single phycoerythrin complexes does not prove the existence of a single quantum system in the sense of a strongly coupled super molecule. In fact, the crystal structure of B-phycoerythrin indicates a relatively week (Forster type) coupling (76). Rather, the photon antibunching is a manifestation of the singlet-singlet annihilation phenomenon within a single complex (73, 77). When a second excitation occurs within an excited complex, the double excitation is quenched via a radiationless relaxation, resulting in one rather than two emitted photons.

One-step photobleaching has been observed on other molecular aggregates. Moreover, under continuous illumination, single aggregate emission switches between on and off states (78, 79). Although similar blinking behavior happens for some single chromophores, such as the GFP discussed earlier, it seems ubiquitous for molecular aggregates. A similar phenomenon has also been observed for semiconductor nanocrystals (80). A detailed study (78) has been conducted by Barbara and coworkers on single conjugated polymers (Figure 14*A*) of

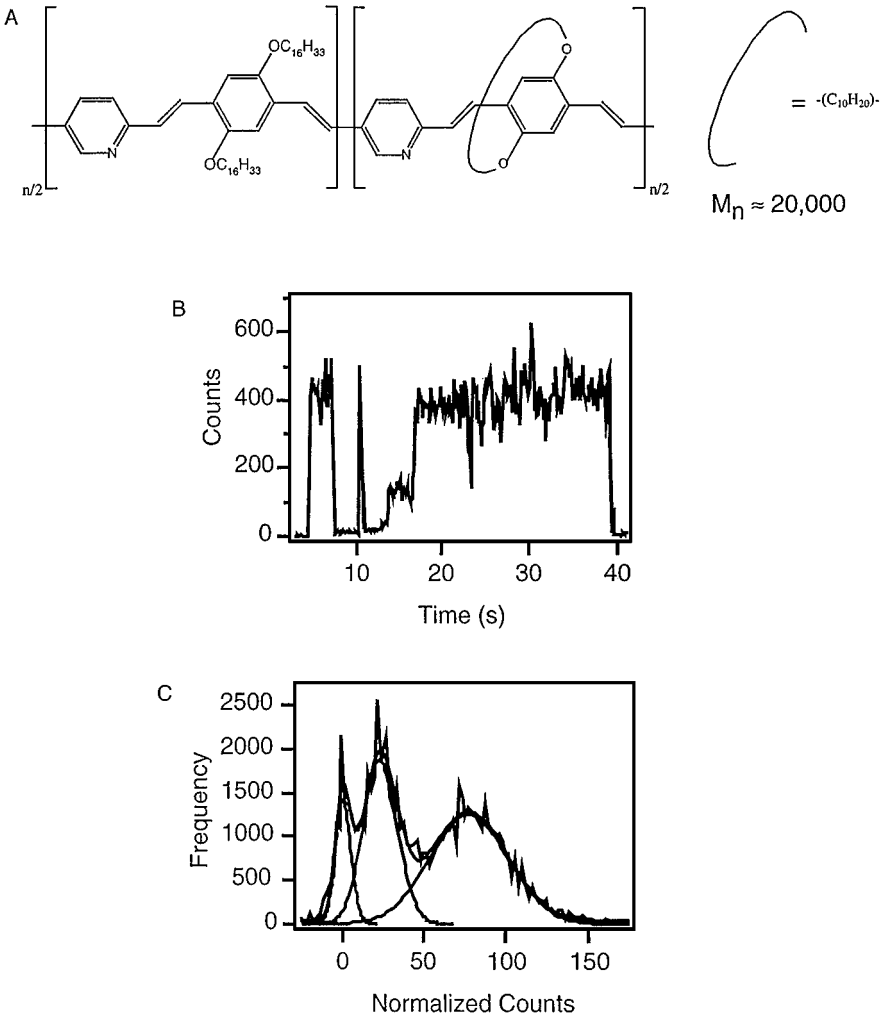

Figure 14 (*A*) Structure of the conjugated polymer molecules studied. (*B*) Intensity trajectory of a single conjugated molecule showing blinking and abrupt photobleaching of the strongly coupled excitonic system. (*C*) A 514-nm excitation histogram of normalized intensity for 40 individual molecules showing dark, intermediate, and bright levels. [Reprinted with permission (78).]

molecular weight ~20,000. Figure 14*B* shows a typical intensity trajectory, and Figure 14*C* shows the histogram of normalized intensity for many individual molecules. The histogram indicates that there are two distinct emitting species, which were proven to have no distinct spectral difference. Independently, another detailed study by Hochstrasser and coworkers (79) has been carried out on the single light-harvesting protein LH-2 from a photosynthetic bacterium, which contains 27 bacteriochlorophyll a chromophores. Besides the off state, several distinct intermediate intensity levels are observed; the fluorescence lifetimes of corresponding species vary. Both groups found the on-time distribution dependent on excitation intensity, which suggests a photoinduced mechanism for generating exciton traps that quench the fluorescence during the off time. The off time was shown to be independent of excitation intensity, which suggests a spontaneous recovery. The exact chemical nature of the exciton traps is unknown. Possible mechanisms include creation of defects via photooxidation for the conjugated polymer (78) and photoinduced electron transfer resulting in bacteriochlorophyll radical cations (79). For a different light harvesting protein, allophycocyanin containing six tetrapyrrole chromophores, Ying & Xie (79a) observed that the generation of radical cation traps is through a two-photon mechanism involving exciton-exciton annihilation. In any case, these photochemical products are usually difficult to observe in ensemble-averaged measurements because of their extremely low quantum efficiencies of formation, but they can be interrogated by repetitive excitations in the single-complex measurements. Research along this line might lead to new insights in material research associated with light-emitting diodes, as well as excitonic interactions in photosynthesis.

CHEMICAL ACTIVITIES

Conventional measurements of chemical kinetics in condensed phases rely on determining concentration changes following rapid mixing of reactants (by stop-flow techniques, for example) or introducing a perturbation (such as temperature jump or photo-excitation). On a single-molecule basis, a chemical reaction, if it occurs, takes place on the sub-picosecond timescale. However, the waiting time prior to such an action, during which the molecule acquires sufficient energy to reach the transition state via thermal activation, is stochastic and long on average. Although single-molecule optical experiments do not have sufficient time resolution to resolve single chemical reactions, the stochastic events of chemical changes can be monitored and the distribution of waiting times can be measured for a single molecule undergoing reversible reactions. Single-molecule chemical reactions can either be repetitively initiated with photo-excitation or occur spontaneously on the ground state, as respectively exemplified below.

Lu & Xie demonstrated single-molecule measurement of photoinduced electron transfer from a sensitizing dye molecule (cresyl violet) to a semiconductor surface (indium-tin-oxide) using repetitive excitation with a picoseond pulse train (81). The fluorescence decay of a single dye molecule reflects the temporal survival probability of the excited state, which, in this case, is dominated by the fast electron transfer from the dye molecule to the conduction band of the semiconductor surface. The decay curve provides a histogram for the waiting times following the laser pulses for the electron transfer to occur on a particular molecule. Previous ensemble-averaged results on similar systems showed multiexponential electron-transfer kinetics. Each single molecule, however, was observed to exhibit a single exponential decay. A broad distribution of site-specific electron transfer rates (10^9–10^{10} s^{-1}) was observed for many single molecules examined. This finding proves that the origin of multiexponential kinetics of electron transfer in this system is the static inhomogeneity of site-dependent electron transfer rates. This and other examples below show that single-molecule kinetics are particularly useful in understanding multiexponential chemical kinetics in inhomogeneous systems.

There has been much interest in studying the chemical activities of single enzyme molecules. Enzymatic activities of individual lactate dehydrogenase (LDH-1) molecules have been investigated by Xue & Yeung (82). In a capillary tube containing a solution of highly diluted enzyme molecules and concentrated substrate molecules [lactate and nicotinamide adenine dinucleotide (NAD^+)], each enzyme molecule produced a discrete zone of thousands of NADH molecules after 1 h of incubation. The zones were then eluted by capillary electrophoresis and monitored by natural fluorescence of NADH. As shown in Figure 15, electrophoretically pure and seemingly identical enzyme molecules show a broad and asymmetrical distribution of activity (threefold), which was otherwise masked by ensemble-averaged measurements. The origin of the distribution in activity was attributed to different conformations of the enzymes. A microscopic picture of the different conformers has yet to appear. The heterogeneity was found to be static on the hour timescale because the same enzyme molecule produces the same zone intensity after another incubation period. Using a similar approach, Craig et al studied single alkaline phosphatase molecules and found an even broader, multipeak distribution of activities (83). The heterogeneity was attributed to glycosylation and other posttranslational modifications, which produce nonidentical copies of enzyme in this system. Temperature-dependence experiments allowed determination of the activation energies of the single enzyme molecules, which vary significantly among molecules. An interesting thermal denaturation experiment on these single enzyme molecules showed that the death of an enzyme, i.e. the loss of enzymatic activity, is abrupt rather than gradual.

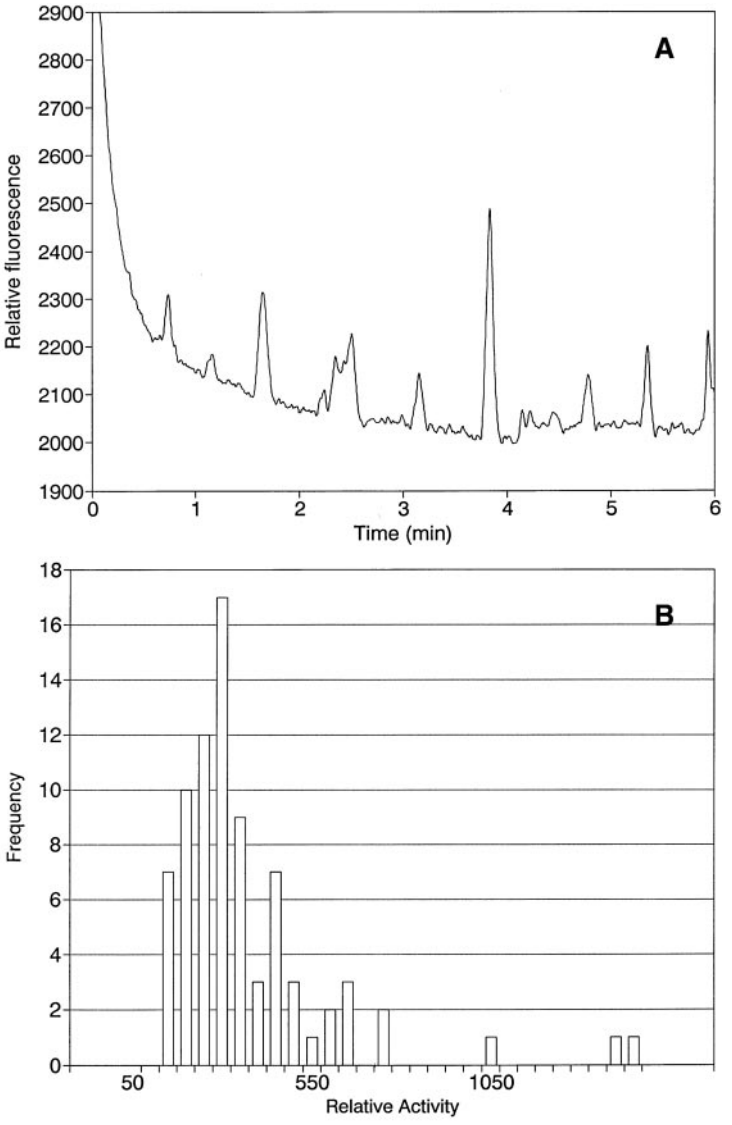

Figure 15 (*A*) Fluorescent zones of NADH molecules, each generated by an individual lactate dehydrogenase (LDH-1) molecule. A dilute solution of LDH-1 (7.6×10^{-17} M) was incubated at 40°C in a 20-μm-diameter capillary tube with 1 mM NAD^+, 3 mM lactate, and 20 mM Tris buffer (pH 9.1) for 1 h. NADH fluorescence at 460 nm was then detected as individual NADH zones were electrophoretically driven through a 305-nm laser focal spot of 10 mm. A variation of integrated areas is observed. (*B*) Histogram of reactivities of single LDH-1 enzyme molecules showing a broad and asymmetrical distribution. [Reprinted with permission (82).]

Although the capillary electrophoresis experiments are particularly effective in identifying heterogeneity of activity, real-time observation of chemical reactions promises to reveal detailed dynamics of enzymatic turnovers. There have been several recent efforts along this line. Yanagida and coworkers first reported visualization of individual ATP turnovers by single myosin molecules, which are molecular motor proteins involved in muscle contraction (20). The single myosin subfragments, S-1 molecules, are tethered on a quartz surface in an aqueous environment, labeled with Cy5 dye, and imaged with total internal reflection excitation and a video rate CCD camera. Cy3-ATP molecules (fluorescent ATP analogue with Cy3 label) are freely diffusing in the solution, giving only a low-fluorescence background signal. When a single Cy3-ATP binds to S-1, the Cy3-ATP emission is localized and intensified at the position of Cy5-S-1. The association-ATP hydrolysis-dissociation process on an individual S-1 molecule was directly monitored in real time with several consecutive fluorescence bursts from single Cy3-ATP molecules at the position of an S-1 molecule. The association appeared to be diffusion controlled, whereas the dissociation time was consistent with the ATP turnover rate in solution, indicating that the fluorescent bursts indeed reflected the ATP turnovers and that the fluorescent labels and substrate immobilization had little influence on the turnover kinetics. Similarly, Vale et al reported direct visualization of movement of single kinesin molecules along microtubules (84), and Sase et al observed axial rotation of sliding actin filaments via polarization imaging of single fluorophores (85).

Lu et al monitored enzymatic turnovers of flavinenzyme molecules in real time by viewing fluorescence from an active site of the enzyme instead of from substrate molecules (86). Cholesterol oxidase, a 53-kDa flavoprotein, catalyzes oxidation of cholesterol by oxygen with the enzymatic cycle shown in Figure 16*A*. The active site of the enzyme, flavin adenine dinucleotide (FAD, Figure 16*B*), is naturally fluorescent in its oxidized form but not in its reduced

Figure 16 (*A*) Enzymatic cycle of cholesterol oxidase, which catalyzes the oxidation of cholesterol by molecule oxygen. The enzyme's naturally fluorescent FAD active site is first reduced by a cholesterol substrate molecule, generating a nonfluorescent $FADH^-$, which is then oxidized by molecular oxygen. (*B*) Structure of FAD, the active site of cholesterol oxidase. (*C*) A portion of the intensity trajectory of an individual cholesterol oxidase molecule undergoing enyzmatic reactions in real time. Each on-off cycle of emission corresponds to an enzymatic turnover. The single cholesterol oxidase is immobilized in agarose gel containing 99% water. The cholesterol concentration is 0.2 mM and the oxygen concentration is 0.25 mM. (*D*) Distribution of emission on-time derived from the intensity trajectory. The nonexponential distribution reflects the fact that the forward reaction involves not an elementary reaction but a kinetic scheme with an intermediate (enzyme-substrate complex). (*solid line*) A curve simulated by convoluting two exponential distributions with $k_1[S] = 2.5\ s^{-1}$ and $k_2 = 15.3\ s^{-1}$ for the kinetic scheme. (Courtesy of HP Lu, Pacific Northwest National Laboratory.)

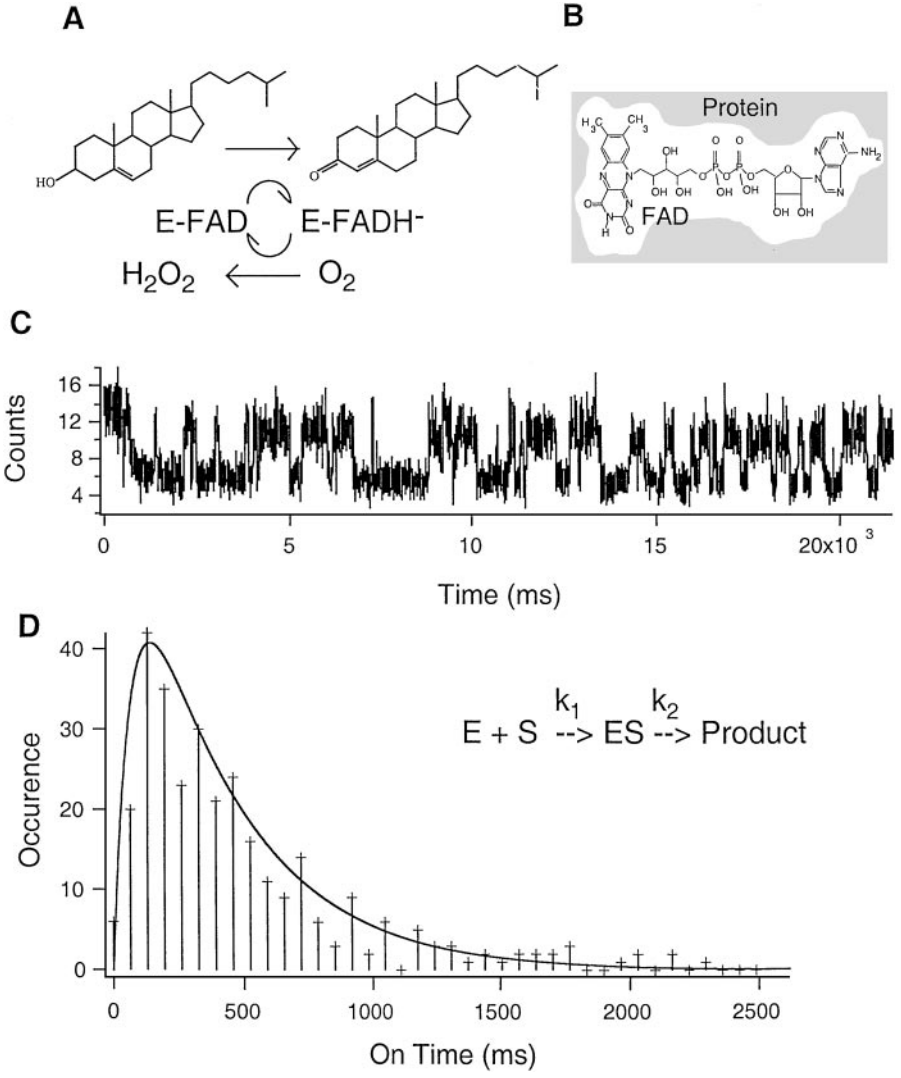

form. Confined in agarose gel containing 99% water, the enzyme molecules are immobilized, yet undergo fast tumbling within the gel, as was proved by a polarization modulation experiment. On the other hand, the small substrate molecules are essentially free to diffuse within the gel. With excess amounts of cholesterol and oxygen molecules, the single FAD emission exhibits on-off behavior (Figure 16*C*), each on-off cycle corresponding to an enzymatic turnover. That on-off cycles required substrate molecules and that the on-off cycles were

independent of the excitation rate proved that the on-off phenomenon indeed originates from spontaneous ground-state enzymatic reactions. The protection of the FAD by the protein matrix results in good photostability of the chromophore, and trajectories of longer than 600 turnovers have been recorded (86).

Statistical analyses of the long turnover trajectories make it possible to test the validity of chemical kinetics at the single-molecule level. For an immobilized single molecule undergoing first-order reversible reactions, with forward and backward rates of k_f and k_b, respectively, the intensity autocorrelation function, $C(t) = \langle \Delta I(0) \Delta I(t) \rangle$, of the fluorescent-reactant molecule is expected to be an exponential decay with a decay rate $k = k_f + k_b$. However, nonexponential $C(t)$ was experimentally observed (86). With the distinct on and off signals in a single-molecule trajectory, forward and backward reactions can be analyzed separately. Similar trajectory analyses have been conducted in patch-clamp studies of single-ion channels (87) and optical-tweezers studies of single molecular motors (88). For an elementary chemical reaction (Poisson process), the distribution of on (or off) time should be an exponential function with a time constant $1/k_f$ (or $1/k_b$). However, a nonexponential distribution has been observed (Figure 16*D*), which is attributed to the complex kinetics scheme associated with the Michaelis-Menton mechanism (86). Moreover, spectral trajectories provide a window on the influence of conformational fluctuations on enzymatic reactions. Similar to the spectral diffusion of dye molecules discussed above, the emission spectrum of an FAD active site fluctuates when no substrate molecules are added, reflecting spontaneous conformational changes at the active site. Interestingly, the spectral fluctuations occur at the timescale of enzymatic turnovers, indicating possible fluctuations of the forward rate. Indeed, such a non-Markovian phenomenon, which is beyond the scope of chemical kinetics, has been observed by statistical analyses of single-molecule trajectories (86). In analyzing single-molecule trajectories Wang & Wolynes pointed out that higher-order correlation functions can yield unique information not obtainable from ensemble-averaged experiments (89, 90).

The major purposes of single-molecule studies of biochemical reactions include the following: (*a*) to measure the distributions of activities and investigate the origin and the fluctuation of the distributions; (*b*) to unravel the reaction mechanisms via statistical analyses of single-molecule trajectories; and (*c*) to observe in real time the transient intermediates that are otherwise difficult to capture in conventional experiments because of their low steady-state concentrations. As usual, well-selected or well-designed experimental observables—such as emission spectra, lifetimes, and FRET—are required for this purpose. The single-molecule methodology is not only informative in physical chemical

studies, it is also expected to be generally useful for biochemistry, molecular biology, and even cell biology.

CONCLUSIONS AND PROSPECTS

The advent of single-molecule detection, imaging, and spectroscopy in ambient environments has stimulated a great deal of activity, so much so that the physical chemistry perspective given in this chapter is only a partial reflection of the field. Nevertheless, even a partial perspective shows that single-molecule methodology is changing the way problems are approached in condensed-phase physical chemistry and that new insights derived from the methodology are beginning to emerge.

The ever-increasing activities in this area have been spurred not only by the wide variety of scientific and technological problems potentially solvable with the single-molecule approach, but also by the ease and relative low cost of the experimental apparatus. The single-molecule fluorescence detection techniques have matured, allowing researchers to apply the technology to, and to focus on, specific problems. Nor will the technological developments stop. UV fluorescence detection, Raman spectroscopy, and nonlinear spectroscopy are likely to broaden the species and spectral identities accessible. Combining optical sensitivity with high-resolution imaging and manipulation techniques, such as atomic force microscopy, the patch clamp technique, and optical tweezers, should prove to be fruitful. Single-molecule methods are being used in efforts to sequence DNA and screen chemical compounds for therapeutic activity.

The single-molecule approach will continue to yield fundamental knowledge on molecular interactions, molecular motions, and chemical kinetics in condensed phase systems. In order to extract new information, it is essential to conduct statistical analyses. If seeing single molecules is almost trivial now, doing fine statistical analyses on trajectories and populations of single molecules requires serious work. Along this line, developments in statistical theory on molecular interactions with nanoenvironments and chemical dynamics pertinent to single-molecule studies will facilitate the experimental efforts. Surface-enhanced Raman also requires theoretical attentions. Further single-molecule photochemical studies will not only shed light on the unknown photoproducts discussed above, they will also discover new and useful photoinduced processes. Many researchers have focused their attention on biomolecules. No doubt one of the most active areas of single-molecule research will be real-time dynamic studies of macromolecular mechanisms: protein folding, allosteric enzyme regulation and signal transductions, and even in vivo observations at natural biological conditions, to name just a few.

Recent advances in room-temperature single-molecule studies have occurred at an extremely rapid pace, often in a surprising manner, generating exciting possibilities in many disciplines. Looking into the future, single-molecule studies will continue to capture the imagination of many scientists for years to come.

ACKNOWLEDGMENTS

We are indebted to many of our coworkers and collaborators. In particular, XSX thanks Peter Lu, Erik Sanchez, Liming Ying, and Luying Xun and JKT thanks John Macklin, Tim Harris, and Louis Brus for their contributions to the work summarized herein. We are also grateful to many of our peers for communicating their results to us. The PNNL work described here has been supported by the US Department of Energy's Office of Energy Research.

Literature Cited

1. Sakamann B, Neher E. 1995. *Single-Channel Recording.* New York: Plenum. 2nd ed.
2. Binnig G, Rohrer H, Gerber C, Weibel E. 1982. *Phys. Rev. Lett.* 49:57–60
2a. Binnig G, Quate CF, Gerber C. 1986. *Phys. Rev. Lett.* 56:930–33
3. Basche T, Moerner WE, Orrit M, Wild UP, eds. 1997. *Single Optical Detection, Imaging and Spectroscopy*. Weinheim: VCH
4. Moerner WE. 1996. *Acc. Chem. Res.* 26:563–71
5. Plakhotnik T, Donley EA, Wild UP. 1997. *Annu. Rev. Phys. Chem.* 48:81–212
6. Xie XS. 1996. *Acc. Chem. Res.* 26:598–606
7. Nie S, Zare RN. 1997. *Annu. Rev. Biophys. Biomol. Struct.* 26:567–96
8. Goodwin PM, Ambrose WP, Keller RA. 1996. *Acc. Chem. Res.* 26:607–13
9. Trautman JK, Ambrose WP. 1997. See Ref. 3, pp. 191–222
10. Dovichi NJ, Chen DD. 1997. See Ref. 3, pp. 223–43
11. Allen MP, Tildesley DJ. 1987. *Computer Simulation of Liquids*. New York: Oxford Univ. Press
12. Shera EB, Seitzinger NK, Davis LM, Keller RA, Soper SA. 1990. *Chem Phys. Lett.* 174:553–57
13. Rigler R, Widengren J, Mets U. 1992. In *Fluorescence Spectroscopy*, ed. OS Wolfbeif, pp. 13–24. Berlin: Springer
14. Barnes MD, Whitten WB, Ramsey JM. 1995. *Anal. Chem.* 67:A418–23
15. Betzig E, Chichester RJ. 1993. *Science* 262:1422–25
16. Trautman JK, Macklin JJ, Brus LE, Betzig E. 1994. *Nature* 369:40–42
17. Xie XS, Dunn RC. 1994. *Science* 265: 361–64
18. Ambrose WP, Goodwin PM, Martin JC, Keller RA. 1994. *Science* 265:364–67
19. Macklin JJ, Trautman JK, Harris TD, Brus LE. 1996. *Science* 272:255–58
20. Funatsu T, Harada Y, Tokunaga M, Saito K, Yanagida T. 1995. *Nature* 374:555–59
21. Schmidt Th, Schutz GJ, Baumgartner W, Gruber HJ, Schindler H. 1995. *J. Phys. Chem.* 99:17662–68
22. Dickson RM, Norris DJ, Tzeng YL, Moerner WE. 1996. *Science* 274:966–98
23. Mertz J, Xu C, Webb WW. 1995. *Opt. Lett.* 20:2532–34
24. Sanchez EJ, Novotny L, Holtom GR, Xie XS. 1997. *J. Phys. Chem.* 101:7019–23
25. Nie S, Emory SR. 1997. *Science* 275: 1102–6
26. Kneipp K, Wang Y, Kneipp H, Perelman LT, Itzkan I, et al. 1997. *Phys. Rev. Lett.* 78:1667–70
27. Betzig E, Trautman JK. 1992. *Science* 257:189–95
28. Trautman JK, Macklin JJ. 1996. *Chem Phys.* 205:221–29

29. Bian RX, Dunn RC, Xie XS, Leung PT. 1995. *Phys. Rev. Lett.* 75:4772–75
30. Novotny L. 1996. *Appl. Phys. Lett.* 69: 3806–8
31. Macklin JJ, Trautman JK. Unpublished
32. Basche Th, Kummer S, Brauchle C. 1995. *Nature* 373:132–34
33. Trautman JK. 1996. In *Proc. Robert A. Welch Found., 39th Conf. Chem. Res.: Nanophase Chemistry*. Houston: Welch Found. Press
34. Ha T, Enderle Th, Chemla DS, Selvin PR, Weiss S. 1997. *Chem. Phys. Lett.* 271:1–5
35. Turro NJ. 1978. *Modern Molecular Photochemistry*. Menlo Park, CA: Benjamin-Cummings
36. Foote CS, Clennan EL. 1995. In *Active Oxygen in Chemistry*, ed. S Foote, JS Valentine, A Greenberg, JF Liebman, p. 105. London: Blackie Acad. Prof.
37. Jones G II. 1990. In *Dye Laser Principles*, ed. FJ Duarte LW Hillman, pp. 287–343. New York: Academic
38. Eggeling C, Brand L, Seidel CAM. 1997. *Bioimaging* 5:105–15
39. Shear JB, Xu C, Webb WW. 1997. *Photochem. Photobiol.* 65:931–36
40. Dickson RM, Cubitt AB, Tsien RY, Moerner WE. 1997. *Nature* 388:355–58

40a. Pierce DW, Hom-Booker N, Vale RD. 1997. *Nature* 388:338

41. Chalfie M, Tu Y, Euskirchen G, Ward WW, Prasher DC. 1994. *Science* 263: 802–5
42. Ha T, Enderle Th, Chemla DS, Selvin PR, Weiss S. 1996. *Phys. Rev. Lett.* 77:3979–82
43. Lu HP, Xie XS. 1997. *Nature* 385:143–46
44. Volker S. 1989. *Annu. Rev. Phys. Chem.* 40:499–530
45. Jankowiak R, Small GJ. 1987. *Science* 237:618–25
46. Friedrich J, Wolfrum H, Haarer D. 1982. *J. Chem. Phys.* 77:2309–16
47. Ambrose WP, Moerner WE. 1991. *Nature* 349:225–27
48. Orrit M, Bernard J. 1990. *Phys. Rev. Lett.* 65:2716–19
49. Myers AB. 1998. *Annu. Rev. Phys. Chem.* 49:267–95
50. Frauenfelder H, Wolynes PG. 1994. *Phys. Today* 47:58–64
51. Moscovits M. 1985. *Rev. Mod. Phys.* 57: 783–826
52. Otto A, Mrozek I, Grabhorn H, Akemann W. 1992. *Phys. Condens. Matter* 4:1143–1212
53. Hildebrandt P, Stockburger M. 1984. *J. Phys. Chem.* 88:5935–44
54. Lee PC, Meisel D. 1982. *J. Phys. Chem.* 86:3391–95
55. Bopp MA, Meixner AJ, Tarrach G, Zschokke-Granacher I, Novotny L. 1996. *Chem. Phys. Lett.* 263:721–26
56. Ruiter AGT, Veerman JA, Garcia-Parajo MF, van Hulst NF. 1997. *J. Phys. Chem. A* 101:7318–23
57. Xu XN, Yeung ES. 1997. *Science* 275: 1106–9
58. Nie S, Chiu DT, Zare RN. 1994. *Science* 266:1018–21
59. Nie S, Chiu DT, Zare RN. 1995. *Anal. Chem.* 67:2849–57
60. Rigler R. 1995. *J. Biotechnol.* 41:177–86
61. Maiti S, Haupts U, Webb WW. 1997. *Proc. Natl. Acad. Sci. USA* 94:11753–57
62. Magde D, Elson E, Webb WW. 1972. *Phys. Rev. Lett.* 29:705–8
63. Chiu DT, Zare RN. 1996. *J. Am. Chem. Soc.* 118:6512–13
64. Ha T, Glass J, Enderle Th, Chemla DS, Weiss S. 1998. *Phys. Rev. Lett.* 80:2093–96
65. Edman L, Mets U, Rigler R. 1996. *Proc. Natl. Acad. Sci. USA* 93:6710–15

65a. Edman L, Mets U, Rigler R. 1995. *Exp. Tech. Phys.* 41:157

66. Wennmalm S, Edman L, Rigler R. 1997. *Proc. Natl. Acad. Sci. USA* 94:10641–46
67. Jia Y, Sytnik A, Li L, Vladimarov S, Cooperman BS, Hochstrasser RM. 1997. *Proc. Natl. Acad. Sci. USA* 94: 7932–36
68. Geva E, Skinner JL. 1998. *Chem. Phys. Lett.* 288:225–9
69. Kubo R. 1961. In *Fluctuation, Relaxation and Resonance in Magnetic Systems*, ed. DT Haar, p. 23. London: Oliver & Boyd
70. Eggeling C, Fries JR, Brand L, Gunther R, Seidel CAM. 1998. *Proc. Natl. Acad. Sci. USA* 95:1556–61
71. Selvin PR. 1995. *Methods Enzymol.* 246: 300–34
72. Ha T, Enderle Th, Ogletree DF, Chemla DS, Selvin P, Weiss S. 1996. *Proc. Natl. Acad. Sci. USA* 93:6264–68
73. Wu M, Goodwin PM, Ambrose WP, Keller RA. 1996. *J. Phys. Chem.* 100: 17406–9
74. Basché Th, Moerner WE, Orrit M, Talon H. 1992. *Phys. Rev. Lett.* 69:1516–19
75. Ambrose WP, Goodwin PM, Enderlein J, Semin DJ, Martin JC, Keller RA. 1997. *Chem. Phys. Lett.* 269:365–70
76. Ficner R, Lobeck K, Schmidt G, Huber R. 1992. *J. Mol. Biol.* 228:935–50

77. van Grondelle R. 1985. *Biochim. Biophys. Acta* 811:147–95
78. Vanden Bout DA, Yip WT, Hu D, Fu DK, Swager TM, Barbara PF. 1997. *Science* 277:1074–77
79. Bopp MA, Jia Y, Li L, Cogdell RJ, Hochstrasser RM. 1997. *Proc. Natl. Acad. Sci. USA* 94:10630–35
79a. Ying L, Xie XS. 1998. *J. Phys. Chem.* Submitted for publication
80. Nirmal M, Dabbousi BO, Bawendi MG, Macklin JJ, Trautman JK, et al. 1996. *Nature* 383:802–4
81. Lu HP, Xie XS. 1997. *J. Phys. Chem. B* 101:2753–57
82. Xue QF, Yeung ES. 1995. *Nature* 373: 681–83
83. Craig DB, Arriaga EA, Wong JCY, Lu H, Dovichi NJ. 1996. *J. Am. Chem. Soc.* 118:5245–53
84. Vale RD, Funatsu T, Pierce DW, Romberg L, Harada Y, Yanagida T. 1996. *Nature* 380:451–53
85. Sase I, Miyata H, Ishiwata S, Kinosita K. 1997. *Proc. Natl. Acad. Sci. USA* 94: 5646–50
86. Lu HP, Xun L, Xie XS. 1998. *Science.* Submitted for publication
87. Colquhoun D, Hawkes AG. 1995. See Ref. 1, pp. 397–482
88. Svoboda K, Mitra PP, Block SM. 1994. *Proc. Natl. Acad. Sci. USA* 91:11782–86
89. Wang J, Wolynes P. 1995. *Phys. Rev. Lett.* 74:4317–20
90. Wang J, Wolynes P. 1998. *J. Chem. Phys.* In press